NIF

NASA

Technical Memorandum 83892

# Spectral Evolution of Active Galactic Nuclei: A Unified Description of the X-ray and $\gamma$-ray Backgrounds



Darryl Leiter and Elihu Boldt


FEBRUARY 1982

National Aeronautics and Space Administration

**Goddard Space Flight Center**
Greenbelt, Maryland 20771

# SPECTRAL EVOLUTION OF ACTIVE GALACTIC NUCLEI: A UNIFIED DESCRIPTION OF THE X-RAY AND $\gamma$-RAY BACKGROUNDS

Darryl Leiter[1] and Elihu Boldt
Laboratory for High Energy Astrophysics
NASA/Goddard Space Flight Center
Greenbelt, Maryland 20771

## ABSTRACT

A model for spectral evolution is presented whereby active galactic nuclei (AGN) of the type observed individually have emerged from an earlier stage at $z \approx 4$ in which they are the thermal X-ray sources responsible for most of the cosmic X-ray background (CXB). We pursue the conjecture that these precursor objects are initially supermassive Schwarzschild black holes with accretion disks radiating near the Eddington luminosity limit. It is noted that after $\sim 10^8$ years these central black holes are spun-up to a "canonical" Kerr equilibrium state ($a/M = 0.998$; Thorne 1974) and shown how they then can lead to spectral evolution involving non-thermal emission extending to gamma-rays, at the expense of reduced thermal disk radiation. A superposition of sources in the precursor stage can thereby account for that major portion of the CXB remaining after the contribution of usual AGN are considered, while a superposition of AGN sources at $z < 1$ can account for the gamma-ray background. Extensive X-ray measurements carried out with the HEAO 1-2 missions as well as gamma-ray and optical data are shown to compare favorably with principal features of this model. Several further observational tests are suggested for establishing the validity of this

scenario for AGN spectral evolution.

Subject headings: black holes - cosmology - galaxies: nuclei - gamma-rays: general - quasars - X-rays: sources - X-rays: spectra

[1]NAS-NRC Senior Research Associate

# I. INTRODUCTION

In this work we present a unified model in which the X-ray and gamma-ray background can result from the superposition of radiation from active galaxies in different stages of their evolutionary history. This scheme is based on the generalization of a black-hole model developed for gamma-ray production in active galaxies (Leiter 1980). It involves both thermal and non-thermal accretion disk processes around supermassive rotating Kerr black-holes. The model has as its main component a canonical Kerr black-hole (specific angular momentum a/M = 0.998; Thorne 1974) assumed to exist at the center of an active galaxy. When surrounded by an accretion disk of hot plasma, this black-hole can generate both X-rays and gamma-rays with high efficiency. The gamma-rays are produced by non-thermal radiation processes associated with the rapid rotation of the black-hole/accretion disk system.

Bignami et al. (1979) have shown that most of the gamma-ray background can be accounted for by a superposition of the non-thermal power-law spectra associated with active galaxies exhibiting spectral breaks in the MeV region, but with no substantial evolution of any sort required. For the X-ray background, DeZotti et al. (1982) have fitted HEAO-1 data within the context of a model based on evolving non-thermal spectra unrelated to known active galaxies which in-toto mimic the thermal spectrum observed. Assuming diffuse emission, Field and Perrenod (1977) have considered that the X-ray background is mainly thermal bremsstrahlung radiation from a hot intergalactic gas (see also Boldt et al. 1979; Marshall et al. 1980; Fabian 1981). Alternately, we have pursued the conjecture that the thermal type spectrum observed in X-rays is itself a basic aspect of the principal individual discrete sources of the X-ray background (Boldt and Leiter 1981). In so doing we have identified a possible evolutionary track for active galaxies whereby the spin-up of a

central massive black-hole (via disk accretion) could lead to a spectral change from that of the thermal emission needed at an earlier epoch for the X-ray background to that of the non-thermal emission required at the present epoch for the gamma-ray background. Such a conjecture has the advantage of eliminating the need for postulating different sources for the X-ray and gamma-ray backgrounds.

## II. THE CXB PROBLEM AND A SOLUTION

Ever since the earliest rocket-borne experiments in X-ray astronomy during the 60's, it has been known that the X-ray sky is dominated by an isotropic background (Giacconi, Gursky, Paolini and Rossi 1962). This situation is almost unique in astronomy. Considering the entire electromagnetic spectrum from MHz radio waves to MeV gamma-rays, the only other band where the isotropic background dominates the sky is that for microwaves, and is well known as due to the $2.7^{0}$ blackbody cosmic background. In contrast, the origin of the X-ray background has remained an open topic, with much speculation (see early reviews by Setti and Rees 1970; Silk 1970). Now, because of recent observations with HEAO-1 and the Einstein Observatory (HEAO-2), there is finally serious expectation of obtaining the detailed information needed for understanding the cosmic X-ray background (CXB) as well. In particular, HEAO-1 has given us a well defined spectrum of the CXB and broad-band spectra of the brightest extragalactic sources (Boldt 1981a) while HEAO-2 has provided us with surveys of dim sources (Giacconi et al. 1979). As pointed out by DeZotti (1980) the CXB spectrum has now been determined to a better precision than the cosmic microwave background spectrum. Up to at least 50 keV or so, the CXB spectrum appears to be that of a thermal plasma at a temperature of a half-billion degrees (Marshall et al. 1980). At photon energies approaching a few hundred keV, much higher than

that associated with kT, this thermal spectrum vanishes and we are left with a low level harder background that extends into the MeV gamma-ray band (see Boldt 1981a).

Can this overall spectrum of background X-rays and γ-rays be synthesized by the superposition of spectra already known for extragalactic sources? In attempting to answer this question we note that in the energy band 3-50 keV, where the comparison must be made most precisely, the information available for individual sources comes mainly from HEAO-1 and is restricted to objects at low redshift. In other words, we have the spectral information required but only for sources in the current epoch. While clusters of galaxies have thermal X-ray spectra, the temperatures involved are an order of magnitude below that associated with the X-ray background (Mushotzky et al. 1978). Furthermore, the X-ray luminosity function for clusters (McKee et al. 1980; Ulmer et al. 1981) implies that they contribute only a few percent of the background, even at the lowest energies. The local luminosity function for X-ray active galaxies is now also well determined, particularly from the recent HEAO-1 work of Piccinotti et al. (1982). Even if we ignore possible evolutionary effects, the implied contribution of such sources to the CXB is about 20% (at ~ 3 keV). By invoking AGN evolution in density and/or luminosity, the contribution at any particular narrow bandwidth of the background could reach 100%. However, we then encounter an apparent paradox in that the broad-band spectra for the many active galaxies measured with HEAO-1 indicate that, for most, they share a spectral form that is clearly different from that of the background. In particular, over the 3-50 keV band they appear as power-law spectra, most of them consistent with a common spectral index (Boldt 1981b; Mushotzky 1982). Those observed at higher energies (Peterson et al. 1981; Rothschild et al. 1981) indicate that this

power-law holds up to at least 100 keV.

Some principal aspects of the extragalactic X-ray sky as defined by the data from HEAO-1 are summarized in Figure 1. What is plotted here is the spectral density for the surface brightness of the CXB as a function of photon energy in keV. This background is here called the "total flux" to indicate that it represents the integral of all unresolved sources. The curve labelled "GSFC" is the best-fit thermal bremsstrahlung spectrum for kT = 40 keV as measured with the HEAO-1 A2 experiment over 3-50 keV by Marshall et al. (1980). The statistical errors involved here are relatively small such that the fit to the data over much of the band is good to within a few percent. The points at higher energies are from preliminary UCSD scintillation counter data obtained by Matteson et al. (1979), and the estimated errors are as indicated.

The power-law labelled "Seyfert galaxies" is an estimate of their total contribution assuming that the population characterized by the local luminosity function is the same as that for all previous epochs since $z \approx 1$. Considering the total flux shown here over the 3-50 keV band as a superposition of two basic spectral components, one of them being a power-law suitable for Seyferts and the other a thermal one, analysis of the HEAO-1 data shows that the power-law component can not exceed 30% (Stottlemyer 1979; DeZotti et al. 1982), referred to $\sim$ 3 keV. This upper limit is only slightly more than the specific power-law spectrum exhibited here, based on the measured luminosity function. Such a power-law component can not be much higher than shown since the dashed line extrapolation to higher energies (see Figure 1) is already comparable to the $\gamma$-ray background; this extrapolation is justified by results on the composite HEAO-1 spectrum for several Seyferts observed up to $\sim$ 100 keV (Peterson et al. 1981; Rothschild et al. 1981). Data

from Apollo 16-17 (Trombka et al. 1978) at higher energies than shown here indicate that the spectrum of the overall background does indeed flatten out into the MeV γ-ray region where it must eventually drop sharply to match SAS-2 data above 30 MeV as obtained by Fichtel, Simpson and Thompson (1978).

For the power-law component shown in Figure 1, most of the flux would come from Seyferts at redshifts less than $z \approx 1$. If we extrapolate HEAO-1 power-law Seyfert spectra down to ~ 1 keV in order to make comparisons with data from the deep exposures obtained with the Einstein Observatory we predict that Seyferts should contribute about 6 detected sources per square degree (Piccinotti et al. 1982) as compared with the actually observed total number of 19 ± 8 per square degree (Giacconi et al. 1979) and that most of these Seyferts would have $z < 1/2$.

If we extrapolate the source count from the Einstein Observatory to objects dimmer than the survey limit we obtain that the number of sources other than Seyferts required to fully account for the background is over $2 \times 10^2$ per square degree (see Appendix B). Since this is larger than the number of bright quasars considered (see Section V), we explore the possibility that another source population is responsible for most of the CXB. Although active galactic nuclei (AGN) in the present epoch have non-thermal power-law spectra unsuitable to the background we pursue the question of whether thermal emission by precursor active galaxies (PAG) leading to AGN could provide us with the required number of objects. Since the effective temperature observed for the residual CXB (see Appendix D) is quite well defined ($30 \text{ keV} > kT \gtrsim 23$ keV), we impose the constraint that these sources have a characteristic proper temperature and that the spread in their redshifts is relatively small. Since these sources at an earlier epoch are here simply taken as precursors of the AGN observed in the present epoch (see Appendix A), their co-moving density

equals that measured for low redshift objects. The number of sources of the CXB resulting from this unified approach (see Appendix B, Figures 7 and 8) is a function of the redshift (z) characteristic of these objects. As discussed in Appendix C, our model is phased to $z \sim 4$. This yields the required number of sources and implies that the proper source temperature is $T \sim (1\text{-}2) \times 10^{9}{}^{o}K$.

This unified description of the extragalactic sky of compact sources involves a model of AGN spectral evolution with specific underlying physical requirements. First, this model must provide a thermostat whereby precursor active galaxies (PAG) are characterized by the appropriate temperature (see Section III). Next, it must also provide a natural switch (see Section IV) which changes the spectrum of the high luminosity thermal PAG sources at high redshift into that of the lower luminosity non-thermal AGN of the present epoch responsible for the gamma-ray background. Finally, it must explain why it is plausible that this evolution starts with the epoch of very young galaxies (see Appendix A for a possible scenario).

## III. ACCRETION DISK THERMOSTAT; PAG SPECTRUM

Lightman (1981) has shown that for optically thin plasmas, a "trans-relativistic" regime exists for which the temperature remains $\lesssim 5 \times 10^{9}$ K over a very large range of density and luminosity parameter space. This range of parameter space is consistent with the physical parameters associated with those of the hot optically thin inner regions (Shapiro, Lightman, and Eardley 1976; Novikov and Thorne 1972) of the PAG accretion disks we envisage (i.e. $M \lesssim 10^{9}\ M_{o}$; $N \gtrsim 10^{9}$ particles/cm$^{3}$; for $L \sim L_{Edd}$, $r < 10^{16}$ cm). This may be interpreted as a thermostatic effect due to the large specific heat associated with the copious $\gamma + \gamma \rightleftharpoons e^{\mp}$ "phase transition" which occurs within this hot optically thin inner region of the accretion disk. For the Eddington

limited accretion disks associated with the PAG (see Figure 2a), the existence of a hot optically thin inner region is assured, but it can also be surrounded by a cooler optically thick disk region which acts as a source of soft photons. In this case the thermostat temperature associated with the "trans-relativistic" regime will be lowered to $\sim 10^9$ K. We can see this effect in Figure 2b where the temperature of the trans-relativistic hot inner region of the disk as calculated by Liang (1979) is plotted against the dimensionless parameter $\ell \equiv [\frac{L_{Edd}}{L} r_{10}/y]$, where $r_{10} \equiv \frac{r(\text{hot inner region})}{(10\ GM/c^2)}$ and y is the Kompaneets parameter associated with the Comptonization of the soft photons. For the PAG characteristic of the CXB, Figure 2b shows that a proper temperature of $T \sim (1\text{-}2) \times 10^9$ K is obtained for the parameter ranges associated with $\log(\ell) = 0 \rightarrow 1$. With $L \sim L_{Edd}$ and $y \simeq 4\ kT/mc^2 \simeq 1$, this corresponds to r(hot inner region) $\lesssim 10^2\ GM/c^2$.

It is important to note that in the presence of disk magnetic fields trapping of $e^{\pm}$ pairs created in the disk could occur. Since protons can be both gravitationally bound as well as being tied to the disk's magnetic field, the $e^{\pm}$ pairs generated by $\gamma + \gamma \rightarrow e^{\pm}$ will be effectively trapped within the disk (i.e., the magnetic field acts like a "spring" between the protons and the pairs) as long as their Larmour radius is less than the radius of the hot inner region. Because this can occur for relativistic $e^{\pm}$ plasmas with magnetic fields exceeding only a few gauss (Lightman 1981), the presence of copious $e^{\pm}$ production within the hot inner region of the disk does not necessarily imply that these particles escape the disk. Rather, it is likely that they remain trapped within the disk, thereby inhibiting any $e^{\pm}$ current flow contribution to disk-dynamo processes which might occur above and below the disk. In this context, the radiated spectrum during the PAG phase would be mostly thermal, with non-thermal disk dynamo processes playing little or no

role.

## IV. AGN SPECTRAL SWITCH: BLACK HOLE SPIN-UP

In the process of the disk accretion associated with radiation, a black hole will eventually be spun-up to a canonical Kerr hole with an equilibrium value of $a/M = 0.998$ (Thorne 1974). This process is traced in Figure 3 where $a^*(x) \equiv a/M$ (specific angular momentum, per unit mass) and the accretion mass-to-energy conversion efficiency $\varepsilon(x)$ are plotted as a function of the ratio $x \equiv M/M_i$, where $M_i$ is the initial Schwarzschild hole mass just prior to disk accretion and M is the hole mass during spin-up. The rate of mass growth for the black hole during this accretion $(\frac{d\ell nx}{dt})$ may be expressed:

$$\theta \frac{d(\ell nx)}{dt} = \left(\frac{L}{L_{Edd}}\right)\left(\frac{1-\varepsilon(x)}{\varepsilon(x)}\right) \qquad (1)$$

where $\theta = 4.5 \times 10^8$ years. Since the equilibrium spin value is achieved when $x \approx 2.5$ (Thorne 1974) and since $L \leq L_{Edd}$ during the spin-up, we can evaluate a lower limit to the duration of time ($\Delta t$) needed for the spin-up by using equation 1 with $\varepsilon(x)$ as shown in Figure 3 and integrating as follows:

$$\Delta t \geq \theta \int_1^{2.5} \left(\frac{\varepsilon(x)}{1-\varepsilon(x)}\right) \frac{dx}{x} \approx 0.2(\theta). \qquad (2)$$

The equality sign in equation (2) corresponds to the case $L = L_{Edd}$ and can be used to estimate the lifetime of the PAG phase, viz $\Delta t \approx 10^8$ years. The canonical state of spin achieved by this time is insensitive to small ($\lesssim 10\%$) perturbations on the disk accretion parameters (Thorne 1974). In this context the evolution of a PAG into a system involving a canonical Kerr hole may be viewed as an essentially irreversible process. Such behavior is of the type needed for describing an evolution whereby the principal sources of the CXB (e.g. PAG objects at $z \approx 4$) lead to the AGN observed at later epochs.

Prior to spin-up, when $a/M \approx 0$, the event horizon for the black hole occurs at $r = 2r_g$ (where $r_g \equiv GM/c^2$), and the inner radius of the accretion disk at $r = 6\ r_g$. As shown in Figure 4 these radii decrease as the black hole increases in spin (Bardeen 1973) and approach their minimal value ($r_g$) when the equilibrium state of a canonical Kerr hole is reached ($a/M = .998$). After $\sim 10^8$ years of accretion (with radiation at the Eddington limit), this maximal penetration of the inner region of the accretion disk causes processes within the ergosphere ($2 > \frac{r}{r_g} > 1$) to be "switched on".

As shown in Figure 5, at spin-up the inner region of the hot ($T \approx 10^9$ K) accretion disk associated with a PAG black hole has effectively penetrated the Penrose target region, causing Penrose Compton Scattering (PCS) of the disk X-rays into MeV $\gamma$-rays (Leiter 1980). These PCS gamma rays are focused into a region within $\sim 40^0$ (above and below) the equatorial plane of the accretion disk. Pair production ($e^{\pm}$) due to $\gamma + X \rightarrow e^{\pm}$ absorption processes occuring between these $\gamma$ -rays and X-rays from the disk create an $e^{\pm}$ plasma wind above and below the disk. Since it is formed outside the disk, this $e^{\pm}$ wind is not trapped by disk magnetic fields and can act to effectively trigger and surge disk dynamo mechanisms (Blandford 1979; Lovelace, MacAuslan and Burns 1979; MacDonald and Thorne 1981) leading to extended structure. The efficiency for energy transfer to the relativistic particles responsible for non-thermal radiation processes (such as synchrotron) can increase appreciably, as the dynamo acceleration region grows (Vestrand et al. 1981; Condon et al. 1981; Cavaliere and Morrison 1980). Eventually, a broad-band of non-thermal radiation can be generated at a high efficiency (Jones 1979), but at the expense of weakened thermal disk emission (Blandford 1979; Lovelace, MacAuslan and Burns 1979; Rees et al. 1982). It is in this way that we account for the

spectral transition from the purely thermal disk X-ray emission associated with PAG to the non-thermal spectra (e.g. synchrotron) of highly relativistic electrons accelerated in Seyfert and QSO sources. In this model the CXB is dominated by PAG and a related class of daughter objects, young quasars (YQSO), which precede QSO and Seyferts in the spectral evolutionary scheme (see Appendix A and Appendix C).

## V. SOURCE PARAMETERS

In order to establish parameters for PAG and YQSO sources we need to make contact with the CXB spectrum observed. As discussed in Appendix D, that portion of the CXB to be identified with such sources may be well represented by a residual CXB spectrum (3-50 keV) of the form

$$\frac{dI}{dE} \propto E^{-\alpha} \exp(-E/kT) \tag{3}$$

where kT can vary from 23 keV for $\alpha$=0 to a maximum value of ~ 30 keV for $\alpha$=0.2. Since most of these sources are here taken to be at a redshift of $z \approx 4$ (see Appendix C), the corresponding characteristic temperature expected at the epoch of source emission may be expressed

$$(kT)_{PAG} \approx (120\text{-}150) \text{ keV}. \tag{4}$$

The sky surface brightness due to such PAG sources is obtained by integrating the spectral solutions exhibited in Appendix D, and leads to a range of values, as follows:

$$I_{PAG} = \int_0^\infty \frac{dI}{dE} dE \approx (1.4 - 1.7) \times 10^{-7} \eta \text{ erg cm}^{-2}\text{s}^{-1}\text{sr}^{-1} \tag{5}$$

where $\eta$ is the fraction of the residual CXB due to PAG (i.e. $(1-\eta)$ is then the fraction of the residual CXB due to YQSO). In evaluating this integral we assume that the solutions of the form given by equation (3) obtained for the 3-50 keV band of the HEAO-1 GSFC data (Appendix D) also hold outside this band. To test this at higher energies we have taken the solution for kT = 30 keV, added it to a baseline spectrum used for known-type sources (see Appendix D) and plotted this semi-empirical model in Figure 1 for comparison with preliminary UCSD data from HEAO-1 (Matteson et al. 1979) at energies $\gtrsim$ 100 keV. Although the crude agreement exhibited is adequate, we note that the UCSD results are being refined (Kinzer et al. 1981). However, a more detailed comparison of the idealized model involved is not warranted.

In order to obtain a measure of PAG source luminosity we make use of the relation

$$I_{PAG} = \frac{c}{4\pi} \int_0^\infty \frac{\bar{L}(t).\rho(t)}{(1+z(t))}\, dt \qquad (6)$$

where t is the light-travel look-back time, $\bar{L}$ is the mean PAG luminosity at t, z is the redshift parameter corresponding to t, $\rho(t)$ is the co-moving density of PAG at t and c is the velocity of light. A fundamental aspect of this model for AGN spectral evolution is that the density of PAG objects in co-moving coordinates remains constant during the time interval of spin-up ($\Delta t \simeq 10^8$ years) and that the co-moving density of AGN after production equals that of the associated PAG objects. This co-moving density is expressed as a dimensionless number $\phi$ representing the ratio of $\rho$ to a value of the density comparable to that measured for local AGN, viz

$$\phi \equiv \rho/(10^{-4}(h_{50})^3(\mathrm{Mpc})^{-3}) \qquad (7)$$

where $h_{50}$ is a measure of the Hubble constant $H_o$ given by $h_{50} \equiv H_o/(50\ km\ s^{-1}\ Mpc^{-1})$. Using $\Delta t = 10^8$ years, $\rho$ expressed via $\phi$ (equation 7) and $I_{PAG}$ given by equation (5), equation (6) yields $\bar{L}_{PAG}$ as a function of z, viz:

$$\bar{L}_{PAG} \approx (5.6\text{-}6.7)\ x10^{45}\ (1+z)n(h_{50})^{-3}\phi^{-1}\ erg\ s^{-1}. \qquad (8)$$

As discussed in Appendix C, we consider that the PAG contribution comes mainly from objects at $z \approx 4$, and therefore

$$\bar{L}_{PAG} \approx 3 \times 10^{46}\ n(h_{50})^{-3}\phi^{-1}\ erg\ s^{-1}. \qquad (9)$$

For $\bar{L}_{PAG} \approx L_{YQSO}$, we estimate (see equation C-11) that $n \gtrsim 0.7$. Assuming that the average radiation efficiency during the spin-up phase defining a PAG is $\langle\varepsilon\rangle \approx 0.2$ (see Figure 3), the accretion rate ($\dot{M}$) corresponding to equation (9) is

$$\dot{M}_{PAG} = 3n(h_{50})^{-3}\phi^{-1}\ M_o/year. \qquad (10)$$

The mass to be associated with the central compact object of the average PAG source of the CXB is obtained from equation (9) under the assumption that the luminosity is at the Eddington limit, viz

$$M_{PAG} = 2 \times 10^8\ n\ (h_{50})^{-3}\ \phi^{-1}\ M_o. \qquad (11)$$

The surface density ($\sigma$) on the celestral sphere of the PAG sources of the CXB discussed here is obtained from

$$\sigma \approx \frac{d\sigma}{d\tau} \Delta\tau \tag{12}$$

where $\tau$ is the look-back time (in units of the age of the universe), $\Delta\tau$ is the $q_0$ dependent interval corresponding to the spin-up time interval $\Delta t = 10^8$ years beginning at $z = 4$ and $\frac{d\sigma}{d\tau}$ is evaluated at $z = 4$ (see Appendix B, Figs. 7 and 8). Considering a range ($0.5 > q_0 > 0$) for the deceleration parameter, equation (12) yields

$$\sigma(\text{PAG}) = (2.0 - 9.7) \times 10^2 \ \phi\ (h_{50})\ \text{deg}^{-2}. \tag{13}$$

The number of sources required for the residual CXB is $\gtrsim 200\ \text{deg}^{-2}$ (Appendix B) and can be satisfied by equation (13) for $q_0 \approx 0.5$ provided $\phi(h_{50}) > 1$. For $q_0$ closer to zero, the required number of sources is more easily satisfied (i.e. with $\phi\ (h_{50}) \approx 1$ or even somewhat less).

Young quasars (YQSO) start out with the mass value attained by a PAG at the end of its lifetime (see Appendix C). This could be somewhat higher than the average PAG mass given by equation (11) and, for nominal values of the parameters indicated, may be bracketed as follows:

$$10^9 > \frac{M_{YQSO}}{M_0} \gtrsim 10^8. \tag{14}$$

The young quasar luminosity is initially Eddington limited, yielding

$$10^{47}\ \text{erg s}^{-1} > L_{YQSO} \gtrsim 10^{46}\ \text{erg s}^{-1}. \tag{15}$$

The beginning of disk-dynamo buildup associated with a young quasar involves the existence of a non-thermal "fireball" effect resulting from the

large value of (L/r) in YQSO (see Appendix C). This dynamo driven "fireball" effect yields a spectrum that, in the X-ray band, can mimic thermal emission at $\sim 2 \times 10^9$K (Cavallo and Rees 1978) during the lifetime of the YQSO. If we assume that the overall radiation efficiency is that of disk emission at spin-up (i.e. $\varepsilon \approx 0.3$), the initial mass accretion rate for the young quasar corresponding to equation (15) would be

$$5 \text{ year}^{-1} > \frac{\dot{M}_{YQSO}}{M_o} \gtrsim 0.5 \text{ year}^{-1}. \qquad (16)$$

However, at $\varepsilon \approx 0.3$ the e-folding time for mass growth (from equation 1) is $\gtrsim 2 \times 10^8$ years and the black-hole mass of a young quasar would be on the order of $10^{10}$ $M_o$ after about $10^9$ years, the characteristic lifetime (see Appendix C). At that stage, the luminosity would no longer be Eddington limited but the mass accretion rate would be supply limited at $\sim 5$ $M_o$ year$^{-1}$, corresponding to a luminosity of $\sim 10^{47}$ erg s$^{-1}$ (see Appendix C). These then would be the values to be associated with the onset of quasar emission, viz

$$\dot{M}_{QSO} \approx 5 \, M_o \text{year}^{-1} \qquad (17)$$

$$L_{QSO} \approx 10^{47} \text{ erg s}^{-1}. \qquad (18)$$

Since $M \approx 10^{10}$ $M_o$ at this QSO stage the Eddington limit exceeds the actual luminosity by an order of magnitude and the compactness parameter (L/r) discussed in Appendix A and Appendix C thereby becomes sufficiently small (i.e. $\lesssim 10^{30}$ erg s$^{-1}$ cm$^{-1}$) for the efficient acceleration of synchrotron radiating relativistic electrons to take place.

As discussed by Bahcall and Soneira (1980) the surface density of quasars

brighter than B=22.5 mag is

$$\sigma(\mathrm{QSO}) \lesssim 50 \ \mathrm{deg}^{-2}. \qquad (19)$$

From the curves exhibited in Figures 7 and 8 the surface density of the associated progenitor YQSO is expected to be about twice that of these bright quasars, essentially independent of $q_0$. Hence, ignoring unrelated YQSO (e.g. short-lived), we assume

$$\sigma(\mathrm{YQSO}) \lesssim 100 \ \mathrm{deg}^{-2}. \qquad (20)$$

Taking the origin for young quasars at z = 4 (hence with $d\sigma/d\tau$ a maximum at z = 4), the peak $d\sigma/d\tau$ for quasars (see Figures 7 and 8) occurs at

$$z(\mathrm{QSO\ peak}) = 2.7 - 3.1 \qquad (21)$$

for $0.5 > q_0 > 0$. This is compatible with recent results (Schmidt and Green 1981; Osmer 1981) indicating a paucity of quasars at $z \gtrsim 3.5$ and offers a plausible explanation for this effect.

Concerning the present phase of the AGN track associated with spiral galaxies (see Appendix A), we note that the mean X-ray luminosity of Seyfert nuclei (Piccinotti et al. 1982) is $\sim 10^{43}$ erg $s^{-1}$. For a radiation efficiency $\varepsilon \approx 0.3$, this corresponds to an accretion rate

$$\dot{M}\ (\mathrm{Seyferts}) \approx 10^{-3}\ M_0\ \mathrm{year}^{-1}\ . \qquad (22)$$

However, the average mass for the central black hole of a Seyfert nucleus would be comparable to the initial mass for the young quasar black hole, viz:

$$10^9 > \frac{M(\text{Seyfert})}{M_\odot} \gtrsim 10^8. \qquad (23)$$

The luminosity is thereby several orders of magnitude below the Eddington limit; therefore the efficient acceleration needed for a synchrotron source is amply allowed. Assuming no evolution in the co-moving density (see Appendix B) we find that, for $0.5 > q_0 > 0$,

$$\sigma(\text{Seyferts};\ z < 1) \approx (4 - 8) \times 10^2\ \phi\ \text{deg}^{-2} \qquad (24)$$

$$\sigma(\text{Seyferts};\ 4 > z > 1) \approx (3 - 14) \times 10^3\ \phi\ \text{deg}^{-2}. \qquad (25)$$

The source parameters specified in this section are summarized in Table 1 "Principal Sources of the Residual CXB" for PAG and young quasars (YQSO) and in Table 2 "Principal Sources of the Non-thermal ($\gamma$-ray) Background" for Seyfert nuclei and quasars (QSO).

TABLE 1

PRINCIPAL SOURCES OF THE RESIDUAL CXB

1. PAG: Precursor Active Galaxies

   a) Sky Brightness: $I = (1.4\text{-}1.7) \times 10^{-7}\ \eta$ erg cm$^{-2}$s$^{-1}$sr$^{-1}$

   b) Lifetime: $\Delta t \approx 10^8$ years

   c) Redshift: $z = 4$

   $\Delta z \approx (0.1\text{-}0.2)h_{50}$ for $0<q_0<.5$ (see Appendix B)

   d) Bolometric

   Luminosity: $\bar{L} = 3 \times 10^{46} \eta (h_{50})^{-3} \phi^{-1}$ erg s$^{-1}$

   e) Eddington Limited

   Accretion Rate: $\dot{M} = 3\eta (h_{50})^{-3} \phi^{-1}\ M_o$ year$^{-1}$

   f) Black hole Mass: $M = 2 \times 10^3\ \eta (h_{50})^{-3}\ \phi^{-1}\ M_o$

   g) Number:

$$4\pi\sigma = \begin{cases} 8.4 \times 10^6\ \phi\ h_{50} & \text{for } q_0 = 0.5 \\ 4.0 \times 10^7\ \phi\ h_{50} & \text{for } q_0 = 0 \end{cases}$$

   h) Hot Inner Region of

   Accretion Disk: { Temperature $T_e \approx (1\text{-}2) \times 10^9$ K
   { Radius $r \lesssim 10^2\ GM/c^2$

2. YQSO: Young Quasars

   a) Sky Brightness: $I = (1.4 - 1.7) \times 10^{-7}\ (1-\eta)$ erg cm$^{-2}$ s$^{-1}$ sr$^{-1}$

   b) Lifetime: $\Delta t \approx 10^9$ years (see App. C)

   c) Redshift: $z \lesssim 4$

   d) Bolometric

   Luminosity: $10^{47}$ erg s$^{-1}$ > $\bar{L}$ (initial) $\gtrsim 10^{46}$ erg s$^{-1}$

e) Eddington Limited

Accretion Rate: $5\ \text{year}^{-1} > \dot{M}\ (\text{initial})/M_0 \gtrsim 0.5\ \text{year}^{-1}$

f) Black hole

Mass: $10^9 > M\ (\text{initial})/M_0 \gtrsim 10^8$

g) Number: $4\pi\sigma \lesssim 4 \times 10^6$

h) Disk Dynamo — Temperature $T_e \approx 2 \times 10^9$ K

Fireball Region: Radius $r \lesssim 10^2\ GM/c^2$

---

Definitions: $\eta \equiv$ fraction of residual CXB due to PAG

$q_0 \equiv$ decleration parameter $H_0 \equiv$ Hubble expansion constant

$h_{50} \equiv H_0/(50\ \text{km s}^{-1}\ \text{Mpc}^{-1})$

$\phi \equiv$ comoving density (unit: $10^{-4}\ (h_{50})^3\ \text{Mpc}^{-3}$)

$G \equiv$ gravitational constant

$c =$ speed of light

TABLE 2

PRINCIPAL SOURCES OF THE NON-THERMAL ($\gamma$-Ray) BACKGROUND

1. Seyfert Nuclei

   a) Luminosity: $\bar{L} = 10^{43}$ erg $s^{-1}$

   b) Supply Limited

      Accretion Rate: $\dot{M} \approx 10^{-3} M_o$ $year^{-1}$

   c) Black hole Mass: $10^9 > M/M_o \gtrsim 10^8$

   d) Lifetime: $\Delta t > 10^{10}$ years

   e) Redshift Limits

      (for $\phi \approx 1$): $z = 0\text{-}4$ (see Figs. 7,8)

   f) Number

      (for $0.5 > q_o > 0$): $4\pi\sigma\ (z < 1) = (2\text{-}3) \times 10^7 \phi$

      $4\pi\sigma\ (z=1\text{-}4) = (1 - 6) \times 10^8\ \phi$

2. Bright Quasars

   a) Luminosity: $\bar{L} = 10^{47}$ erg $s^{-1}$

   b) Supply Limited

      Accretion Rate: $\dot{M} \approx 5 M_o$ $year^{-1}$

   c) Black hole Mass: $M \approx 10^{10} M_o$

   d) Lifetime: $\Delta t \approx 10^9$ years (see App. C)

   e) Redshift (at maximum $\frac{d\sigma}{d\tau}$):

      $z(\text{peak}) = 2.7\text{-}3.1$ (for $0.5 > q_o > 0$;

      see Figs. 7,8)

f) Number (brighter than B = 22.5 mag)

$$4\pi\sigma \lesssim 2 \times 10^6$$

---

Definitions: $q_0 \equiv$ deceleration parameter $H_0 \equiv$ Hubble expansion constant

$h_{50} \equiv H_0/(50 \text{ km s}^{-1} \text{ Mpc}^{-1})$

$\phi \equiv$ comoving density (unit: $10^{-4}(H_{50})^3 \text{ Mpc}^{-3}$)

## VI. FURTHER OBSERVATIONAL TESTS

Are X-ray sources such as the PAG and young quasars postulated here among the objects detected with the HEAO-2 Einstein Observatory? In the deep surveys discussed by Giacconi et al. (1979) the sample considered corresponded to extragalactic sources with $S_E > 2.6 \times 10^{-14}$ erg cm$^{-2}$s$^{-1}$ (1-3 keV). For comparison, the PAG sources characterized in Table 1 would have intensities in the 1-3 keV band given by

$$S(\text{PAG}) = (0.4 - 2.1) \times 10^{-14}\, \eta (h_{50})^{-1} \phi^{-1} \text{ erg cm}^{-2}\text{s}^{-1} \qquad (25)$$

for $q_0 = 0$-$0.5$. Since we expect that $\eta (h_{50})^{-1} \phi^{-1} \lesssim 1$, equation (25) shows that these sources would not be well represented in the sample considered complete, but that some of the dimmest unidentified objects detected should be considered candidates. However, the increased sensitivity and bandwidth planned for the Advanced X-ray Astrophysics Facility (AXAF) telescope (Weisskopf 1981) should be sufficient for the study of a substantial sample of PAG.

The X-ray detectability for young quasars appears more promising with respect to data already available. Although the distribution of young quasars is here taken to peak at $z \approx 4$, as shown in Figures 7 and 8, their surface density still exceeds that of the peak for quasars at $z \approx 3$ and does not fall below quasars until $z \lesssim 2$. For the thermal X-ray spectrum considered, the flux expected in the HEAO-2 1-3 keV band from a source at $z = 2$ is given by

$$S(z=2) = (0.8 - 1.9) \times 10^{-14} (h_{50})^2 L_{46} \text{erg cm}^{-2}\text{s}^{-1} \qquad (26)$$

where the limits correspond to $q_0 = 0 \rightarrow 0.5$ and $L_{46}$ is the bolometric

luminosity of the source in units of $10^{46}$ erg $s^{-1}$. Since $(h_{50})^2 L_{46} \gtrsim 1$ for young quasars, they could be well represented in the Einstein Observatory (HEAO-2) deep surveys. In particular, the observed sample of quasar candidates with $z \gtrsim 2$ would be dominated by what we refer to as young quasars.

How can we tell young quasars from quasars optically? Extrapolating from X-rays (> 1 keV) to the UV (<< 1 keV) the non-thermal quasar spectrum should generally be steeper than the thermal type continuum of the young quasar. Hence, line emission from regions around the source excited mainly by UV radiation (see Davidson and Netzer 1979) would be relatively weak for young quasars. However, the need for some X-ray excitation has been considered (Shields and Mushotzky 1979; Kwan and Krolik 1979, 1981); in particular Grindley et al. (1980) emphasize that X-rays could be the major energy input to the broadline regions (BLR) of radio quiet quasars. In such a case, the young quasars might be characterized by substantial BLR emission but little or no emission from narrow line regions (NLR). Since NLR radiation may be absent for quasar candidates observed with BLR emission at $z > 2$ (Ferland 1981), these objects could qualify as young quasars, and a separate model for their line emission warrants further investigation.

Since the X-ray spectrum for a young quasar (or PAG) is a thermal type, its proper characterization would require a large bandwidth (i.e. $\Delta E \gtrsim kT$). For a young quasar at $z \approx 2$, a bandwidth as high as ~ 100 keV would be required for an unambiguous determination but is technically difficult for such a dim source. While future focusing X-ray telescopes (Serlemitsos 1981; Weisskopf 1981) with bandwidths approaching 10 keV will still not identify the exponential roll-off at > 10 keV characteristic of such spectra, they would nevertheless be sufficient for establishing that the spectral index at $\lesssim 10$ keV is substantially smaller (i.e. flatter spectrum) than that characterizing

Seyfert nuclei (and quasars, if such be the case).

Although our scenario for the evolution of young quasars into quasars and their subsequent extinction provides an idealized description of these events (see Appendix C), some qualitative features emerge which are fundamental observables. In particular, we note three regimes to be associated with quasar evolution, viz:

1) For $z < 1$ the evolution is dominated by an exponential increase in the comoving number density with look-back time (i.e. density evolution characterized by $\kappa \approx 10$ for the lowest luminosity bright quasars) since the most luminous radio quiet quasars with lifetimes shorter than about a billion years have already decayed away. The relatively weak evolution and high luminosity observed for radio loud quasars (Schmidt 1978) could be indicative of a large accretion reservoir (up to $\sim 10^{10}$ $M_0$) to be associated with young elliptical galaxies.

2) For $z \gtrsim 1$, the increase in number with look-back time is more rapid for higher luminosity quasars (Schmidt and Green 1980). We associate this with the correspondingly faster exhaustion of the mass reservoir available for powering the higher output by accretion. In this regime, the evolution is then essentially that of luminosity.

3) For $z \gtrsim 2$ (see Figures 7 and 8) the number of young quasars relative to quasars increases rapidly with look-back time and the evolution is dominantly of a spectral nature (i.e. thermal type emission of young quasars as compared with the supposed synchrotron type emission of quasars). This leads to a rapid decrease in the number of quasars expected between $z \approx 3$ and $z \approx 4$, consistent with recent results (Osmer 1981; Schmidt and Green 1981).

For the track associated with spiral galaxies we expect little or no evolution of any kind after the Seyfert phase begins (see Appendix A, Figures

7 and 8). In particular, the comoving density of Seyfert nuclei should be observed as essentially constant for redshifts up to $z \lesssim 4$. As discussed in Appendix A, most of the evolution (i.e. luminosity and spectral) occurs within the relatively short time associated with the transition of spiral PAG (Eddington limited thermal emission) to Seyfert nuclei (supply limited non-thermal emission).

In general, the temporal variability for massive compact objects is limited by the light travel time across the Schwarzschild radius such that

$\Delta t > \frac{2GM}{c^3} = 3\ M_9$ hours, where $M_9$ is the mass in units of $10^9\ M_\odot$. For the sample of over 30 bright AGN observed with HEAO-1 by Tennant et al. (1981), only one showed strong X-ray variability on timescales less than 3 hours. This negative result is consistent with a central compact mass not much less than $M_9 \approx 1$ for most AGN within the present epoch, but definitive work on the dominant timescale for any variability characterizing this sample as a whole is still needed.

The gamma-ray emission from AGN could have two different components within the context of the model presented. The first component would be the transient Penrose Compton Scattered (PCS) gamma-rays at $\lesssim 3$ MeV associated with $e^{\pm}$ injection phases for the dynamo synchrotron source (Leiter 1980); see Section IV. The second component would consist of the continuous gamma-radiation emitted in a (SSC) synchrotron self-Compton process (Jones, O'dell and Stein 1974) by the relativistic electrons accelerated by the disk-dynamo system. The gamma-ray background observed by Fichtel, Simpson and Thompson (1978) at $E \gtrsim 35$ MeV is here identified with this second component and, as such, gives us the high energy tail of the composite spectrum of SSC radiating Seyfert nuclei. The composite spectrum of these Seyfert nuclei at

much lower energies (i.e. E < 100 keV) may also be attributed to the SSC process (Mushotzky and Marshall 1980). In so doing, we can relate the spectral index for the power-law observed in X-rays with the steeper index observed for gamma-rays (at $\gtrsim$ 35 MeV). In particular, Tucker (1967) relates the index well above the break $\alpha'$ to the optically thin radio synchrotron spectral index $\alpha$ by

$$\alpha' = \frac{4}{3}\alpha + 1 \qquad (27)$$

where he has assumed no injection of new particles and no re-isotropization of pitch angles. Equation (27) is to be associated with the case of intermittent impulsive injection of charged particles. This is to be contrasted with the situation of continuous injection and acceleration where

$$\alpha' = \alpha + \frac{1}{2}. \qquad (28)$$

For the SSC model of X-ray emission, the spectrum is a power-law with the same index as that which describes synchrotron radio emission by the corresponding population of electrons. Since the X-ray spectra for Seyfert nuclei are power laws of energy index $\alpha \approx 0.6 \rightarrow 0.7$ (Boldt 1981b; Mushotzky 1982) equation (28) may be used to estimate $\alpha' = 1.1 \rightarrow 1.2$ as the smallest index possible for the power-law expected well above the energy where the spectrum breaks. Under the conjecture that the gamma-ray background at $\gtrsim$ 35 MeV measured with SAS-2 (Fichtel, Simpson and Thompson 1978) is due mainly to Seyfert galaxies, the observed $\alpha' = 1.7$ (+0.4, - 0.3) would be somewhat larger than the minimum predicted by a synchrotron-type model. However, the situation for impulsive injection described by equation (27) would require $\alpha' = 1.8 \rightarrow 1.9$, in good

agreement with the index observed, suggesting that the synchrotron radiating electrons are indeed replenished via a mechanism involving bursts.

Although the gamma-ray background is still relatively uncertain, Webber, Lockwood and Simpson (1981) have renewed the suggestion that there may be an "excess component" or "bump" in the spectrum in the region of a few MeV. If such is the case, we would want to test that it may be associated with the PCS gamma-rays discussed earlier. Since these gamma-rays are from transient events, this excess component of the gamma-ray background would exhibit temporal variability; the burst characteristic of a PCS event is of duration $\Delta t \gtrsim M_9$ days, with a spectral break at $\lesssim 3$ MeV (Leiter 1980).

Observations of the Seyfert galaxies NGC 4151 and MCG 8-11-11 by Perotti et al. (1979, 1981a, 1981b) indicate that these objects are indeed gamma-ray sources up to at least a few Mev. However, a spectral break could exist at higher energies since these sources were not detected with SAS-2 (Bignami et al. 1979). Furthermore, NGC 4151 may exhibit temporal variability in MeV gamma rays (Perotti et al. 1981a; White et al. 1980). As discussed by Perotti et al. (1981b), the gamma ray flux in the MeV region from these sources is so high (when "on") that any conjecture whereby they are representative of the Seyfert population as a whole would imply that the duty cycle for such gamma radiation is only on the order of a percent. If the duty cycle were much higher, Seyfert galaxies would overproduce the gamma-ray background in the MeV region. On the other hand, a $\sim$ 1% duty cycle is consistent with the PCS gamma ray production process (Leiter 1980) inherent in our model of AGN evolution for Seyferts since the canonical Kerr black hole required is stable to small (< 10%) perturbations (Thorne 1974).

Quasars are not expected to yield observable PCS gamma rays since this radiation would be absorbed by accretion disk X-rays via $X + \gamma \rightarrow e^{\mp}$ processes

(i.e. the X-ray luminosity of quasars is not sufficiently small compared with the Eddington limit). Since the source of these $\gamma$-rays is the PCS target region (see Figure 5) within the ergosphere (i.e. $1 < r/r_g < 2$) the compactness parameter (L/r) for quasars would be much larger than the maximum value ($\sim 10^{30}$ erg $s^{-1}$ $cm^{-1}$) permitted for avoiding such extreme $\gamma$-ray absorption (Cavaliere and Morrison 1980). For Seyfert galaxies, the luminosities involved are generally less than a percent of the Eddington limit (for the black-hole mass values considered here), and the compactness parameter for the PCS source region could thereby be sufficiently small for the PCS gamma rays to escape.

In addition to the search for bursts of PCS gamma rays ($\lesssim$ 3 MeV) from individual Seyfert galaxies, the proposed model for the background would suggest that the effect of such bursts should be most evident from an observation of temporal variability in the "excess component" of the gamma-ray background. Since this background is here taken to be dominated by Seyferts, the relevant number of sources (see Table 2) is that for $z < 1$; viz: $\sigma \lesssim 7 \times 10^2$ $deg^{-2}$. If the effective duty cycle for observable PCS gamma-radiation is on the order of a percent, then the number of Seyferts exhibiting a burst during an observing time $\Delta t \lesssim 1$ day would be $\sigma(\text{with burst}) \lesssim 7$ $deg^{-2}$. An example of a practical experiment for detecting the associated background variability would be one where observations are restricted to small pixels of the sky (e.g. 10 $deg^2$) and flux measurements compared for data accumulated over several intervals separated by $\Delta t > 1$ day. For this example, the temporal fluctuations per pixel in the excess component of the gamma-ray background would be $\gtrsim$ 12% (i.e. $\gtrsim 1/\sqrt{70}$). If the photon flux in the excess component is $\gtrsim 10^{-2}$ $cm^{-2}s^{-1}sr^{-1}$ (Webber, Lockwood and Simpson 1981) the count accumulated in a day would be $\gtrsim 3$ $cm^{-2}$ per pixel. Using a detector area

of $\sim$ 50 $cm^2$, the statistical error associated with this measurement could be $\lesssim$ 8% (i.e. $1/\sqrt{150}$). The Compton telescope planned for the Gamma Ray Observatory (GRO) satellite mission (Kniffen 1981) should be an appropriate instrument for carrying out such an experiment since it would not be dominated by extraneous background counts, and the effective area (at $\lesssim$ 3 MeV) and angular resolution appear adequate.

The detection of temporal variability of the sort described in an excess gamma-ray component would be strong evidence that this background is indeed due mainly to active galactic nuclei (at $z < 1$) associated with supermassive canonical Kerr black holes. Such variability would imply that the "excess" $\sim$ MeV component of the $\gamma$ -ray background could not be predominantly cosmological in origin, as previously considered (Brown and Stecker 1979).

Confirmation of these proposed observational tests for AGN spectral evolution would offer strong evidence in support of the original conjecture by Lynden-Bell (1969) that accretion of matter onto a supermassive black hole is indeed the source of power for the AGN phenomenon.

## ACKNOWLEDGMENTS

We thank Alan Stottlemyer for data analysis associated with HEAO-1 (A2) measurements of the X-ray background. One of us (D.L.) acknowledges the hospitality and encouragement provided by Reuven Ramaty and the Laboratory for High Energy Astrophysics.

# APPENDIX A

## A FRAMEWORK FOR AGN SPECTRAL EVOLUTION

We explore a scenario for AGN spectral evolution (Boldt and Leiter 1981) which begins with the postulate that the supermassive black-holes which lead to PAG are generated and evolve toward masses up to $\sim 10^9 M_0$ by pregalactic processes beginning at $z > 100$ (Carr 1980). While the massive black holes involved might well have been produced as primordial objects in the radiation dominated era, we will consider the effects of their presence starting at the recombination era in order to make contact with possible galactic space-time correlations such as needed for our model. Since the supermassive black-holes considered are present at recombination, they can act as seeds to aid protogalaxy formation at later epochs (Ryan 1972; Carr 1977). At the epoch of galaxy formation, these protogalactically correlated black-holes are expected to acquire accretion disks and thereby generate PAG. Disk accretion during an earlier phase is absent; this implies that the thermal X-ray emission from PAG is directly phased with the redshift value characeristic of protogalaxy formation. As discussed in Appendix C, the PAG model for the CXB is characterized by $z \approx 4$, consistent with such a protogalactic correlation.

We note that prior to the formation of accretion disks, random pregalactic processes which involve spherical accretion are not expected to be efficient for X-radiation (Brinkmann 1980). Therefore, we conclude that the X-radiation associated with accretion would be relatively unimportant until galaxy formation processes supply the matter associated with an ample accretion disk. Furthermore, pregalactic processes associated with random accretion should not cause appreciable spin-up of the black holes because the capture cross-section for negative angular momentum particles (i.e. opposite to the hole's spin) is greater than that for positive angular momentum

(Ruffini and Wheeler 1975). Beginning at $z \approx 4$, within the epoch of galaxy formation, these supermassive black holes could acquire significant accretion disks for the first time and become the "seeds" which distinguish PAG from galaxies which will evolve normally.

The PAG model for AGN spectral evolution may be described via two idealized evolutionary tracks, one associated with spiral galaxies and the other with elliptical galaxies (see Figure 6). The PAG objects leading to Seyfert nuclei are here taken to involve spiral galaxies (Adams 1977), where the amount of mass available for accretion from a low angular momentum configuration (e.g. in the central bulge) is not large compared with that of the initial massive pregalactic black-hole (i.e. $\lesssim 10^9$ $M_\odot$). As pointed out by Thorne (1974), the spin-up of a black-hole via a radiating accretion disk reaches an equilibrium "canonical" value ($a/M \approx 0.998$) when the hole's mass increases by $\Delta M \approx 1.5$ M (initial). Hence, for the spiral PAG track we expect that a luminosity as high as $\sim 10^{47}$ erg $s^{-1}$ (i.e. Eddington limit for $10^9$ $M_\odot$) could not last much beyond spin-up. After the central bulge supply is exhausted, the accretion rate is limited by the high angular momentum configuration of the remaining gas, located in the extended spiral disk of the galaxy, and any further growth of the central black-hole is relatively minor. In support of this idea we note that the amorphous nature of the spiral galaxies associated with Seyfert nuclei may well be caused by a process which slowly feeds material from outer regions into the center (Simkin, Su and Schwarz 1980). For such a situation, the AGN resulting from the spiral PAG track readily survive to be observed in the present epoch (i.e. as Seyfert nuclei) with luminosities ($\sim 10^{43}$ erg $s^{-1}$) several orders of magnitude below the Eddington limit but with non-thermal spectra extending well into the gamma-ray band (see Section IV).

The PAG leading to quasars (radio loud) are here taken to involve galaxies where the amount of mass available for accretion from a low angular momentum configuration is large (i.e. $> 10^9 M_0$) compared with that of the initial massive pregalactic black hole, but where a high angular momentum reservoir (i.e. such as needed for long-term "slow feeding") is essentially absent. In this situation the luminosity could remain near the Eddington limit for a relatively long time beyond the PAG duration of $\sim 10^8$ years (see Section IV) required for spin-up but would then vanish in $\lesssim 10^{10}$ years as the mass available for accretion finally became exhausted. The morphology of the underlying galaxies involved would probably be elliptical, although direct evidence supporting this is still inconclusive (Hutchings et al. 1981). However, if radio quiet quasars are mainly associated with spiral galaxies, then we would expect their high luminosity stage to be necessarily short-lived ($\lesssim 10^9$ years) followed by a steady state of low luminosity (e.g. such as Seyfert nuclei).

By the end of the PAG phase the central massive object has become a spun-up "canonical Kerr hole", and ergospherically induced electron-positron injection (see Section IV) can trigger and surge electromagnetic disk-dynamo mechanisms. However, as discussed by Cavaliere and Morrison (1980), the efficiency for energy transfer to the relativistic particles responsible for non-thermal radiation processes (e.g. synchrotron) will begin to increase appreciably only when the compactness parameter ($L/r \equiv$ luminosity/radius) for the source falls below $\sim 10^{30}$ erg $s^{-1}$ $cm^{-1}$. For sources with $r \lesssim 10^2\ r_g$ ($r_g \equiv GM/c^2 = 1.5 \times 10^5\ M/M_0$ cm), this will not happen until the luminosity corresponds to much less than the Eddington limit ($L_{Edd} \equiv 1.3 \times 10^{38}\ M/M_0$ erg $s^{-1}$), by at least an order of magnitude. Hence, we expect that there will be a class of young AGN which are not yet sufficiently efficient

non-thermal disk-dynamo sources to be readily identified as quasars while their X-ray luminosity is still close to the Eddington limit. Since these AGN precede quasars (QSO) in this evolutionary scheme, we identify them as (YQSO) young quasars (see Appendix C) with spectra undergoing transition. For the elliptical PAG track we expect that this evolution may readily proceed to completion, in the order: PAG, YQSO, QSO (radio quiet) to QSO (radio loud) with extended structure. For the spiral PAG track, on the other hand, the compactness parameter diminishes by orders of magnitude not long after the PAG phase (i.e. corresponding to the large drop in luminosity caused by the reduction of accretion rate to the steady low-level associated with Seyferts) and YQSO may often proceed directly to Seyferts, bypassing the QSO stage. When QSO do occur in the spiral track they are likely to be relatively short-lived and thus restricted to the radio quiet phase. Ignoring these intermediate phenomena there would then be two principal spectral states (clearly distinct) to be associated with the spiral PAG track, one connected with the thermal disk emission of the PAG and the other with the non-thermal (e.g. synchrotron) emission by relativistic electrons accelerated via the black hole disk-dynamo of Seyfert nuclei. The evolution of two such idealized tracks is summarized in Figures 7 and 8, where the surface density of AGN per unit look-back time is traced as a function of look-back time (see Appendix B), considered separately for Seyferts and quasars.

The assumption that most Seyfert nuclei involve a supermassive black hole with $M/M_0 \approx 10^8$-$10^9$ implies that this class of AGN is characterized by a small compactness parameter (i.e. $L/r < 10^{30}$ erg $s^{-1}$ $cm^{-1}$) and that rapid variability ($\lesssim$ minutes) would be absent. Gamma ray emission from Seyferts would suggest that the compactness parameter characteristic of these sources is indeed small (Bassani and Dean 1981). Rapid variability is extremely rare

(Tennant et al. 1982). The pronounced rapid variability observed for NGC 6814 by Tennant et al. (1981) is very unusual for a Seyfert nucleus; for this particular source $M \lesssim 10^7 M_\odot$ and $L/r \approx 10^{30}$ erg $s^{-1}$ $cm^{-1}$. It is possible that rare Seyfert-like objects such as NGC 6814 are to be associated with low duty cycle recurrent activity for galactic nuclei (Sanders 1981) where the central object involved is much less massive than the pregalactic black holes we have associated with most Seyferts. Hence, such objects could not be part of the PAG evolutionary track we have considered.

## APPENDIX B

## THE COUNT OF MASSIVE COMPACT OBJECTS

In tracing the evolution of massive pregalactic black holes into active galactic nuclei we invoke a conservation law whereby the comoving density ($\phi$) of these objects remains constant. Their change of identity occurs during the relatively short duration ($\Delta t \sim 10^8$ years) of the PAG transition phase. In Figures 7 and 8 we exhibit the corresponding object count on the celestral sphere as a function of the light-travel lookback time ($\tau$) as measured in units of the Hubble time ($H_0^{-1}$ for $q_0 = 0$ and $\frac{2}{3} H_0^{-1}$ for $q_0 = 1/2$). We denote the surface density of objects on the celestrial sphere as $\sigma(\text{deg}^{-2})$ and construct $\frac{d\sigma}{d\tau}$ as follows:

$$\frac{d\sigma}{d\tau} = \left(\frac{d\sigma}{dz}\right) \frac{dz}{d\tau} \tag{B1}$$

where we have used the apparent distance as expressed by Terrell (1977) to evaluate $d\sigma/dz$ (Weinberg 1972), viz

$$\frac{d\sigma}{dz} = \frac{A}{(1+z)^3} \frac{\phi\, z^2}{(2q_0\, z+1)^{1/2}} \left[1 + \frac{z\,(1-q_0)}{((1+2q_0 z)^{1/2}+1+q_0 z)}\right]^2 \tag{B2}$$

with $A = 6567$ deg$^{-2}$ and the comoving density expressed by the dimensionless number $\phi$ (see equation (7)) giving the value in units of $10^{-4}\ (h_{50})^3\ (\text{Mpc})^{-3}$, where $h_{50}$ is a dimensionless measure of the Hubble constant $H_0$, given by

$$h_{50} \equiv H_0/(50\ \text{kms}^{-1}\ \text{Mpc}^{-1}). \tag{B3}$$

In so doing we have normalized to a comoving density that is comparable to the local density of active galaxies observed (Simkin, Su and Schwartz 1980; Boldt

1981a; Piccinotti et al. 1982). The two cases considered correspond to limiting values for the decleration parameter (i.e. $1/2 > q_0 > 0$), viz:

$$\left(\frac{dz}{d\tau}\right)_0 = (1 + z)^2 \tag{B4}$$

$$\left(\frac{dz}{d\tau}\right)_{1/2} = \frac{2}{3}(1 + z)^{5/2}. \tag{B5}$$

The epoch for the PAG transition is phased to occur at $z = 4$ (see Appendix C), corresponding to $\tau = 0.80$ (for $q_0 = 0$) and $\tau = 0.91$ (for $q_0 = 1/2$).

For the evolution of Seyfert nuclei, their co-moving density is here taken, to first approximation, as remaining strictly constant all the way from PAG to the present epoch ($\tau = 0$), thus ignoring possible intervening YQSO (QSO) phases in the associated spiral galaxies. In effect this corresponds to assuming a Seyfert evolution time that is not small compared with a Hubble time. Although the comoving density remains constant during the PAG phase for the quasar track considered here as well, we assume that once young quasars are produced (i.e. at the time of spin-up to a canonical Kerr black hole) they begin to evolve into the corresponding non-thermal sources (i.e. optically bright quasars) by a process which we describe as a transformation from young quasar (parent) to quasar (daughter) characterized by a transition probability rate $\lambda_1$ for the young quasar co-moving density, viz:

$$-\frac{d\phi}{dt} = \lambda_1 \phi. \tag{B6}$$

As discussed in Appendix C, we assume that $\lambda_1$ is comparable to the constant ($\kappa$) value used to characterize the evolution of quasar comoving density as an exponential in look back time, such that

$$\lambda_1 = \kappa \tag{B7}$$

where $\kappa = 10$ (Schmidt 1978). The curves exhibited in Figures 7 and 8 correspond to the following prescriptions for the associated comoving density:

$$\phi \text{ (Massive Pregalactic B.H.)} = 1 \text{ for } z > 4, \text{ (0 for } z < 4). \tag{B8}$$

$$\phi \text{ (Seyfert Nuclei)} = 1 \text{ for } z < 4, \text{ (0 for } z > 4). \tag{B9}$$

$$\phi \text{ (Young Quasars)} = \begin{cases} \exp(\kappa(\tau - 0.80)) & \text{for } z < 4 \ (q_0 = 0). \\ \exp(\kappa(\tau - 0.91)) & \text{for } z > 4 \ (q_0 = 0.5). \\ 0 & \text{for } z > 4. \end{cases} \tag{B10}$$

$$\frac{\phi \text{ (Quasars)}}{\phi \text{ (Young Quasars)}} = \begin{cases} \kappa(0.80 - \tau) & \text{for } q_0 = 0 \\ \kappa(0.91 - \tau) & \text{for } q_0 = 0.5 \end{cases} \quad (\text{where } \kappa = 10) \tag{B11}$$

The points shown in Figures 7 and 8 for PAG correspond to $\phi$ (PAG) = 1. Although such a normalization for the PAG associated with spiral galaxies allows for values of $\frac{d\sigma}{d\tau}$ which are numerically compatible with direct observations of Seyfert nuclei at $\tau = 0$ it leads to an apparent overproduction of quasars when taken as the normalization for the PAG associated with YQSO/QSO (e.g. in elliptical galaxies). This implies that, for the track leading to bright quasars, the correct value for the comoving density of the corresponding PAG objects is less than the value used for Figures 7 and 8. For bright quasars (Bahcall and Soneira 1980) $\sigma \lesssim 50$ deg$^{-2}$, which implies that the associated PAG galaxies should be normalized

by $\phi(\mathrm{PAG}) \lesssim 8 \times 10^{-2}$ for $q_0 \lesssim 1/2$.

The total number of sources required for the CXB to be identified with objects such as PAG (and young quasars) may be estimated in terms of the number of extragalactic sources detected with the Einstein Observatory (HEAO-2). For a survey limit of $S_E(1\text{-}3\ \mathrm{keV}) = 2.6 \times 10^{-14}$ erg cm$^{-2}$ s$^{-1}$, the detected sources correspond to $\sigma_E = 19 \pm 8$ deg$^{-2}$ (Giacconi et al. 1979). Assuming a Log N-Log S relation of slope (a) near the survey limit, the total surface density on the celestial sphere ($\sigma_p$) required for objects such as PAG is given by

$$\frac{\sigma_p}{\sigma_E} = f^{(1-\Gamma)}(I_p/I_E)^{\Gamma} \qquad (312)$$

where f is the fraction of HEAO-2 sources that are PAG (and young quasars), $I_p$ is the CXB intensity due to PAG, $I_E$ is the CXB intensity due to all sources brighter than $S_E$ and

$$\Gamma \equiv a/(a-1). \qquad (B13)$$

Taking $I_p \approx 3\ I_E$ at $\lesssim 3$ keV and $a < 2.3$ (the slope used by Green and Schmidt (1978) for optically bright quasars), these equations yield

$$\frac{\sigma_p}{\sigma_E} > 7\ f^{-0.8}. \qquad (B14)$$

However, a substantial portion of the sources detected with the HEAO-2 deep survey are probably objects that are relatively nearby (Fabian 1981). For example, based upon the local luminosity function for Seyfert galaxies and clusters of galaxies as measured with HEAO-1, Piccinotti et al. (1982)

estimate that the number expected within the HEAO-2 survey is ~ 6 $deg^{-2}$ for Seyferts and ~ 1 $deg^{-2}$ for clusters, assuming no evolution. And most of these sources would correspond to $z < 0.5$. The remaining sources detected might be mainly quasars (Cavaliere et al. 1981). Hence, it appears rather safe to assume $f < 0.5$. Using equation (B14) this corresponds to $\sigma_p > 230$ $deg^{-2}$ as compared to the upper limit (Bahcall and Soneira 1980) for optically bright quasars (i.e. $\sigma \lesssim 50$ $deg^{-2}$). Therefore, in order for PAG objects to be the dominant sources of the CXB their number must exceed that of optically bright quasars. For a PAG lifetime $\Delta t \approx 10^8$ years, $(\frac{d\sigma}{d\tau})$ as evaluated with equations (B1-B5) at z=4 implies that the corresponding surface density (see eq. (12)) is

$$\sigma_p = (2.0\text{-}9.7) \times 10^2 \ \phi \ h_{50} \ deg^{-2} \qquad (B15)$$

for $0.5 > q_0 > 0$. Since $h_{50} \gtrsim 1$, the condition that $\sigma_p > 230$ $deg^{-2}$ could be met with $\phi \approx 1$.

# APPENDIX C

## YOUNG QUASARS

For redshifts where most optically bright quasars have been observed ($1/2 < z < 2$) their evolution may be described in terms of a comoving density that varies exponentially in lookback time ($\tau$), as follows

$$\phi \propto \exp(+\kappa\tau) \qquad (C1)$$

where $\kappa \approx 10\text{-}24$ (Schmidt and Green 1980). To match observations at higher redshifts (Osmer 1981; Schmidt and Green 1981) requires that the co-moving density for such quasars must flatten and reach a maximum value at a redshift $z \approx 3$ ($\tau \gtrsim 0.75$), vanishing at $z \gtrsim 3.5$. These then are the principal constraints which our model for quasar production and lifetime must satisfy.

When the supermassive black hole associated with a PAG has been spun-up to a canonical Kerr black hole the luminosity is initially near the Eddington limited value, viz

$$L \approx 1.3 \times 10^{47} M_9 \text{ erg s}^{-1} \qquad (C2)$$

where $M_9 \equiv 10^{-9} M/M_\odot$. Under such conditions the compactness parameter L/r (luminosity/radius) for the source is so large that the energy losses for relativistic electrons due to inelastic particle production processes are too rapid for the efficient formation of a non-thermal synchrotron radiator (Cavaliere and Morrison 1980). Therefore, the objects so produced can not be the bright quasars we are looking for but do qualify as supermassive black-hole dynamo counterparts of the transient fireball sources discussed by

Cavallo and Rees (1978). The fireball lifetime is then identifiable with the lifetime of the young quasars considered here.

When do young quasars evolve into quasars? For $L \lesssim 10^{-1} L_{Edd}$, a synchrotron source can begin to operate efficiently (i.e. the compactness parameter can become sufficiently small), and the young quasar can thereby become a quasar. When the accretion rate is supply limited, the luminosity can level off even though the mass of the black hole continues to increase. We then evaluate $L/L_{Edd}$ via equation (1), as follows:

$$L/L_{Edd} = \frac{\varepsilon}{(1-\varepsilon)} \left(\frac{\dot{M}}{M}\right) \theta \qquad (C3)$$

where $\theta = 4.5 \times 10^8$ years and we take $\varepsilon \approx 0.3$ for an AGN. Equation (C3) shows that, after $(\dot{M})$ is supply limited, $(L/L_{Edd})$ will decrease as (M) grows. In particular, we find that by the time the quasar condition $L/L_{Edd} \lesssim 10^{-1}$ is satisfied, the characteristic time for further growth $(M/\dot{M})$ has lengthened to $\gtrsim 2 \times 10^9$ years. Since a luminosity $\sim 10^{47}$ erg $s^{-1}$ (such as for a quasar) would require an accretion rate $\sim 5\ M_0$ year$^{-1}$ the corresponding increase in the black hole mass ($\Delta M \gtrsim 2 \times 10^9$ years $\times$ 5 $M_0$ year$^{-1}$) would be $\gtrsim 10^{10}\ M_0$. On the other hand, when the initial mass available for accretion is $\sim 10^{10}\ M_0$ the quasar lifetime would thereby be limited to $\lesssim 2 \times 10^9$ years.

We are now ready to construct a model for the evolution in the comoving density of quasars. Taking $\lambda_1$ as the parent-daughter transition rate from young quasars (YQSO) to quasars (QSO) and $\lambda_2$ as the disappearance rate for quasars (i.e. lifetime = $1/\lambda_2$), we obtain

$$\phi(\text{YQSO}) = [\phi(\text{PAG})] \exp(-\lambda_1 \Delta\tau) \qquad (C4)$$

$$\phi(QSO) = \frac{\phi(PAG)\lambda_1}{\lambda_2 - \lambda_1} [\exp(-\lambda_1 \Delta\tau) - \exp(-\lambda_2 \Delta\tau)] \qquad (C5)$$

where $\phi(PAG)$ is the comoving density of the associated PAG and

$$\Delta\tau \equiv \tau(PAG) - \tau \qquad (C6)$$

where $\tau$ is the light travel lookback time in units of the Hubble time.

For $\tau$ sufficiently small (i.e. low z) we must have $\phi(QSO) > \phi$ (YQSO). This then implies that $\lambda_2 \lesssim \lambda_1$. From the discussion following equation (C3) we expect $\lambda_2 \approx \lambda_1$ (corresponding to $\lambda^{-1} \lesssim 2 \times 10^9$ years); in such a case equation (C5) becomes

$$\phi(QSO) \approx \phi(PAG)\lambda_1 \, \Delta\tau \, \exp(-\lambda_1 \Delta\tau) \qquad (C7)$$

and reaches a maximum at $(\Delta\tau)_m$ given by

$$(\Delta\tau)_m = (\lambda_1)^{-1}. \qquad (C8)$$

For $\Delta\tau > \lambda_1^{-1}$, the evolution in the quasar comoving density is dominated by the exponential behavior and we recover the observed form (C1) required by making the identification

$$\lambda_1 = \kappa. \qquad (C9)$$

For $\kappa \approx 10\text{-}24$, equations (C8) and (C9) imply that $(\Delta\tau)_m \approx (0.4\text{-}1) \times 10^{-1}$, corresponding to an e-folding time $\lesssim 2 \times 10^9$ years (for $q_0 \gtrsim 0$, $h_{50} \gtrsim 1$), comparable to the lifetime estimated via equation (C3). Since the redshift at

which the quasar comoving density is a maximum is required to be at $z \approx 3$, we may use equations (B4) and (B5) with (C8) to infer that this is offset from the PAG origin by $\Delta z \approx 1$, for $1/2 > q_0 > 0$. This then fixes the PAG epoch at a redshift $z(PAG) \approx 4$.

The relative contributions of PAG at $z \approx 4$ and young quasars (YQSO) at $z \approx 3$ to the CXB may be estimated as

$$\frac{\eta}{1-\eta} \gtrsim 0.4 \frac{\sigma(PAG)}{\sigma(YQSO)} \cdot \frac{L(PAG)}{L(YQSO)}. \qquad (C10)$$

For $\sigma(PAG) \gtrsim 6 \times 10^2 \ (h_{50}) \ \phi \ deg^{-2}$ (corresponding to $q_0 \lesssim 0.05$), $\sigma(YQSO) \lesssim 10^2$ $deg^{-2}$ and $L(PAG) \approx L(YQSO)$ we use equation (C10) to obtain

$$\frac{\eta}{1-\eta} \gtrsim 2 \ (h_{50}) \ \phi. \qquad (C11)$$

With $(h_{50}) \ \phi \gtrsim 1$, we use equation (C11) to infer that $\eta \gtrsim 0.7$.

# APPENDIX D

## CXB RESIDUAL SPECTRUM

The CXB spectrum as measured with HEAO-1 (Marshall et al. 1980) over the band 3-50 keV may be well fit with an isothermal bremsstrahlung model corresponding to an optically thin hot plasma at kT ≈ 40 keV. However, the thermal spectra for clusters of galaxies correspond to temperatures that are almost an order of magnitude cooler (Mushotzky et al. 1978) and Seyfert galaxies exhibit spectra that are clearly non-thermal (Rothschild et al. 1981). Since the local X-ray luminosity functions for clusters (McKee et al. 1980) and Seyfert galaxies (Piccinotti et al. 1982) have recently been well determined with the same HEAO-1 experiment used to measure the CXB, the spectral baseline for the residual CXB can now be reliably estimated. The contribution of optically bright quasars may also be estimated (Cavaliere et al. 1981), but this has been restricted to the 1-3 keV band of HEAO-2 and involves a spectral extrapolation to much higher energies in order to make contact with the region addressed here. Based on a 20% contribution from Seyferts (Marshall et al. 1980; Boldt 1981; Piccinotti et al. 1982) and a 4% contribution from clusters (Hintzen et al. 1980) at 3 keV, the CXB surface brightness arising from known sources ($dI_s/dw$) is taken as

$$(dI_s/dw)/B = 0.10(w^{-\alpha_1}+w^{-\alpha_2})\ (1-\beta+\beta\exp(-w^{-3})) + 0.05\ w^{-.5}\exp\left[\frac{(1-w)}{w_T}\right] + 0.24(1.5w)^{-\gamma} \qquad (D1)$$

where

$$w \equiv E/(3\ \text{keV}),$$

B is the spectral density at 3 keV for the total CXB (B =5.2 $cm^{-2}$ $s^{-1}$ $sr^{-1}$), $\alpha_1$ and $\alpha_2$ are limits on the energy spectral index for Seyferts, $\beta$ is a dimensionless parameter characterizing the self absorption effects on the Seyfert spectra near 3 keV, $w_T$ characterizes the energy for the thermal emission from clusters of galaxies (we take $w_T$ = 2.3 corresponding to T = 8 x $10^{7o}$ K) and $\gamma$ is the energy spectral index for bright quasars, with the constraint that their contribution equals 20% of the CXB as extrapolated to the 1-3 keV band (Cavaliere et al. 1981).

Seyfert galaxies form a homogeneous class of objects as regards X-ray spectrum (Mushotzky et al. 1980). Regardless of X-ray luminosity or optical line structure (i.e. broad or narrow), the broad-band X-ray spectra of Seyfert galaxies are always power-laws with the same energy spectral index (Boldt 1981b; Mushotzky 1982) $\alpha \approx 0.6$-$0.7$; hence we take $\alpha_1 = 0.6$, $\alpha_2 = 0.7$. High luminosity Seyferts ($>> 10^{43}$ erg $s^{-1}$ for E < 10 keV) show no evidence for significant self-absorption (Lawrence and Elvis 1982). However, the X-ray luminosity function is steep (Piccinotti et al. 1982) and about half the local volume emissivity due to Seyfert galaxies arises from sources with luminosities less than $10^{43}$ erg $s^{-1}$. Absorption effects seem to be commonly associated with low luminosity Seyferts such as NGC 4151, where the column density of material covering about 90% of the source corresponds to unit optical depth at ~ 3 keV (Holt et al. 1980). We consider that a fraction $\beta < 0.5$ of the volume emissivity for Seyferts is associated with photoelectric absorption (i.e. cross-section varying as $w^{-3}$) corresponding to unit optical depth at 3 keV and that this is the sole distortion of the power-law spectra of these sources. The HEAO-2 source count for Seyferts requires absorption effects corresponding to $\beta \gtrsim 6 \times 10^{-2}$ (Fabian, Kembhavi,

and Ward 1981).

As for quasars, our spectral knowledge of the X-ray emission is meager. The only broad-band spectrum measured for a radio-quiet quasar is that for QSO 0241+622 obtained with HEAO-1 (Worrall et al. 1980) and may be characterized by an energy spectral index $\gamma = 0.9$. Since the CXB spectrum probably steepens below 3 keV (Garmire and Nousek 1981), however, most quasar X-ray emission might be similar to that of BL Lac type objects, where a steep spectral component (with $\gamma \approx 1.4$) is common (Holt 1980; Worrall et al. 1981). Therefore, we assume $\gamma = 0.9 - 1.4$, subject to the constraint that the contribution of bright quasars to the background is 20% (1-3 keV), as discussed by Cavaliere et al. (1981). Although the total quasar contribution within the 1-3 keV band could be as high as 30% (Kembhavi and Fabian 1981) the uncertainty in the contribution at the much higher energies considered here would still be dominated by the unknown spread in the $\gamma$ to be used for the extrapolation.

Using a baseline spectrum given by equation (D1), characterized by $\beta = (0,0.5)$ and $\gamma = (0.9,1.4)$, we have used HEAO-1 data on the CXB to obtain the residual spectra exhibited in Figure 9. The four residual spectra considered are multiplied by exp(E/23 keV) in order to compare them with the spectral form

$$\frac{dI}{dE} \propto \exp(-E/(23\ \text{keV})). \qquad (D2)$$

For the parameter values considered, the goodness of fit seems to change significantly only at the lowest energies (< 5 keV), where there is some indication favoring $\beta \approx 0$, $\gamma \approx 0.9$. For the bulk of the spectrum, the average value (i.e. the horizontal line) provides a decent fit to the data for all the

four cases exhibited, suggesting that the exact value assumed for $\gamma$ is not critical in this range.

We have also considered the more general thermal spectral form given by

$$\frac{dI}{dE} \propto E^{-\alpha} \exp(-E/kT). \qquad (D3)$$

For $kT \gtrsim 23$ keV, the fit to the data is comparable to that obtained with equation (D2) when $\alpha$ is prescribed by

$$\alpha \approx 0.8\ (1-(23\ \text{keV}/kT)) \qquad (D4)$$

provided that $\alpha < 0.2$. Hence, isothermal fits to the data are acceptable up to $kT \approx 30$ keV. However, a spread in temperatures is also permitted. For example, the superposition of an isothermal spectral component at $kT = 33$ keV with another isothermal component at $kT = 13$ keV (normalized at 3 keV) yields a composite spectrum that is an approximately isothermal one characterized by $kT = 23$ keV to an accuracy that is sufficient for matching the residual CXB observed (3-50 keV).

## FIGURE CAPTIONS

Figure 1 - The surface brightness spectral density of the extragalactic X-ray sky as a function of photon energy. The curve indicating total flux is the best-fit thermal spectrum (kT = 40 keV) for the total extragalactic X-ray background measured with the GSFC instrument (Marshall et al. 1980). The dashed line extension of this curve to energies above 50 keV corresponds to a model involving the superposition of the estimated contributions (see text) from Seyfert galaxies, quasars (with $\gamma = 0.9$) and a thermal component (kT = 30 keV) consistent with the residual spectrum at lower energies (3-50 keV). The UCSD data points shown correspond to preliminary results (Matteson et al. 1979) from HEAO-1 scintillator measurements of the background. The power-law spectrum represents the composite flux from Seyfert galaxies with $z < 1$, based on spectral data from the GSFC HEAO-1 sample of individual sources (Mushotzky 1981; Boldt 1981b) and the associated luminosity function (Piccinotti et al. 1982; Boldt 1981), assuming no evolution.

Figure 2a - A schematic cross-section of a PAG accretion disk surrounding its central supermassive black hole. The hot bloated inner region generates a hard X-ray luminosity $L_X$(PAG) via Comptonization of the soft photon luminosity $L_{soft}$ emanating from the cooler outer regions of the disk.

Figure 2b - A plot of the logarithm of $T_{MAX}$, in the hot trans-relativistic inner region of the (PAG) accretion disk, versus the logorithm of the parameter $\ell \equiv [(L_{Edd}/L)\ r_{10}/y]$. Here $r_{10} \equiv (r/10\ \frac{GM}{c^2})$ is the radius of the hot inner region of the disk, $L/L_{Edd}$ is the Eddington ratio associated with the luminosity in hard X-rays, and y is the Kompaneets parameter for the Comptonization of soft photons into hard X-rays.

Figure 3 - A plot of the PAG black hole specific angular momentum per unit mass $a^*(x)$ and the PAG accretion mass-to-energy efficiency $\varepsilon(x)$ versus the parameter $x \equiv (M/M_i)$ where $M_i$ is the initial mass of the pregalactic supermassive black-hole at the beginning of accretion disk formation.

Figure 4 - The inner radius of the PAG accretion disk and the event horizon of its massive central black hole (units of $r_g \equiv GM/c^2$) versus the black hole specific angular momentum per unit mass $a/M$ (see Bardeen 1973).

Figure 5 - A schematic representation of the nonthermal spectral switching mechanism for the central engine of an AGN. At spin up to a "canonical Kerr black hole" ($a/M \approx .998$) the hot $T \sim 10^9$ K inner region of the PAG accretion disk has amply penetrated the ergosphere, initiating Penrose Compton Scattering of accretion disk X-rays ($\gtrsim$ 50 keV) into $\lesssim$ 3 MeV $\gamma$ -rays beamed into a region extending $40^0$ above and below the accretion disk. These ergospherically generated $\gamma$-rays can produce $e^{\pm}$ pairs via interactions with accretion disk X-rays, thereby forming a copius $e^{\pm}$ plasma wind above and below the accretion disk, as shown.

Figure 6 - A schematic representation for the evolution of massive pregalactic black holes into active galactic nuclei (AGN), according to a scenario presented in Appendix A. The formation of precursor active galaxies (PAG) and their ultimate evolution into quasars (radio loud) and Seyfert nuclei is traced by following the cosmological arrow of time (generated by the expansion of the universe) along the two idealized tracks indicated. Intervening short-lived YQSO (QSO) are omitted.

Figure 7 - The surface density of massive compact objects per unit light-travel lookback time ($\frac{d\sigma}{d\tau}$) as a function of $\tau$, lookback time expressed in units of ($H_0^{-1}$) for $q_0 = 0$. Representative values of the corresponding redshift parameter (z) are indicated along the top scale. The curves exhibited for massive pregalactic black holes, Seyfert nuclei and young quasars are all normalized to the value of ($\frac{d\sigma}{d\tau}$) at $z = 4$ ($\tau = 0.80$) indicated for precursor active galaxies (PAG) during their relatively brief lifetime ( $\Delta\tau \approx 3.6 \times 10^{-3}$ $(h_{50})$). The point shown for PAG corresponds to a co-moving density $\phi$ (PAG) = 1 (unit $\equiv 10^{-4}$ $(h_{50})^3$ $Mpc^{-3}$). See Appendix B.

Figure 8 - The surface density of massive compact objects per unit light-travel lookback time ($\frac{d\sigma}{d\tau}$) as a function of $\tau$, lookback time expressed in units of ($\frac{2}{3} H_0^{-1}$), for $q_0 = 1/2$. Representative values of the corresponding redshift parameter (z) are indicated along the top scale. The curves exhibited for massive pregalactic black holes, Seyfert nuclei and young quasars are all normalized to the value of ($\frac{d\sigma}{d\tau}$) at $z = 4$ ($\tau = 0.91$) indicated for precursor active galaxies (PAG) during their relatively brief lifetime ($\Delta\tau \approx 5.4 \times 10^{-3}$ $(h_{50})$). The point shown for PAG corresponds to a co-moving density $\phi$ (PAG) = 1 (unit $\equiv 10^{-4}$ $(h_{50})^3$ $Mpc^{-3}$). See Appendix B.

Figure 9 - The residual energy spectrum for the CXB multiplied by exp(E/23 keV) as a function of photon energy (E). The points shown correspond to GSFC measurements carried out with a xenon proportional chamber designated HED-1 (High Energy Detector #1) of the HEAO-1 (A2) experiment during 1977: Days 318-357. The offset used for this spectrum corresponds to the superposition of the contributions estimated (see Appendix D) for Seyfert galaxies (with

low-energy absorption characterized by $\beta$ ) and quasars (with energy spectral index $\gamma$ ). In general, the statistical error bars associated with the data points increase with energy and are indicated only for points at ~ 5 keV, ~ 10 keV and those above 20 keV. Horizontal lines correspond to the average value of the associated points plotted. Data points for the incident X-ray intensity were obtained from the raw multichannel pulse height spectrum by using individual channel efficiencies determined by folding the best-fit analytical input spectrum (Marshall et al. 1980) through the calibrated response function of the detector.

## REFERENCES


Adams, T.F. 1977, Ap. J. Suppl. 33, 19.

Bahcall, J., and Soneira, R. 1980, Ap. J. 238, L17.

Bardeen, J. 1973, in "Black Holes" (edited by C. and B.S. DeWitt), Gordon and Breach, New York, p. 225.

Bassani, L. and Dean, A.J. 1981, Nature 294, 332.

Bignami, G., Fichtel, C., Hartman, R., and Thompson, D. 1979, Ap. J. 232, 649.

Blandford, R.D. 1979, in "Active Galactic Nuclei" (edited by C. Hazard and S. Mitton), Cambridge University Press, p. 241.

Boldt, E., Stottlemyer, A., Shafer, R., Holt, S., Rothschild, R., and Serlemitsos, P. 1979, "(COSPAR) X-ray Astronomy" (edited by W. Baity and L. Peterson), Pergamon Press, Oxford and New York, p. 449.

Boldt, E. 1981a, Comments on Astrophysics 9, 97.

Boldt, E. 1981b, Proceedings, Wash. Acad. of Sci. 71, 24.

Boldt, E., and Leiter, D. 1981, Nature 290, 483.

Brinkmann, W. 1980, Astr. Ap. 85, 146.

Brown, R., and Stecker, F. 1979, Phys. Rev. Lett. 43, 315.

Carr, B.J. 1977, Astr. Ap. 56, 377.

Carr, B.J. 1980, Nature 284, 326.

Cavaliere, A., and Morrison, P. 1980, Ap. J. 238, L63.

Cavaliere, A., Danese, L., DeZotti, G., and Franceschini, A. 1981, Astr. Ap. 97, 269.

Cavallo, G., and Rees, M. 1978, M.N.R.A.S. 183, 43.

Condon, J., O'Dell, S., Puschell, J. and Stein, W. 1981, Ap. J. 246, 624.

Davidson, K., and Netzer, H. 1979, Rev. Mod. Phys. 51, 715.

De Zotti, G. 1980, Second International Krakow School of Cosmology, Jablonna,

Poland.

De Zotti, G., Boldt, E., Cavaliere, A., Danese, L., Franceschini, A., Marshall, F., Swank, J., and Szymkowiak, A. 1982, Ap. J., in press, Feb.

Fabian, A. 1981, Proceedings of Tenth Texas Symposium On Relativistic Astrophysics (Baltimore, 1980), Ann. N.Y. Acad. of Sci 375.

Fabian, A., Kembhavi, A., and Ward, M. 1981, 15th ESLAB Symposium on X-ray Astronomy, Amsterdam.

Ferland, G. 1981, private communication.

Fichtel, C., Simpson, G., and Thompson, D. 1978, Ap. J. 222, 833.

Field, G., and Perrenod, S. 1977, Ap. J. 215, 717.

Garmire, G., and Nousek, J. 1981, Bull. AAS 12, 853.

Green, R.F., and Schmidt, M. 1978, Ap. J. 220, L1.

Giacconi, R., Gursky, J., Paolini, F. and Rossi, B. 1962, Phys. Rev. Lett. 9, 439.

Giacconi, R. et al. 1979, Ap. J. 234, L1.

Grindley, J., Steiner, J., Forman, W., Canizares, C., and McClintock, J. 1980, Ap. J. 239, L43.

Hintzen, P., Scott, J., and McKee, J. 1980, Ap. J. 242, 857.

Holt, S., Mushotzky, R., Becker, R., Boldt, E., Serlemitsos, P., Szymkowiak, A., and White, N. 1980, Ap. J. 241, L13.

Holt, S. 1980, NASA TM 82010.

Hutchings, J., Crampton, D., Campbell, B. and Pritchet, C. 1981, Ap. J. 247, 743.

Jones, T. 1979, Ap. J. 233, 796.

Jones, T., O'Dell, S. and Stein, W. 1974, Ap. J. 188, 353.

Kembhavi, A., and Fabian, A. 1981, Ap. J., in press.

Kinzer, R. et al. 1981, in preparation.

Kniffen, D. 1981, private communication.

Kwan, J., and Krolik, J. 1979, Ap. J. 233, L91; 1981, Ap. J. 250, 478.

Lawrence, A. and Elvis, M. 1982, Ap. J. (in press).

Leiter, D. 1980, Astr. Ap. 89, 370.

Liang, E.P.T. 1979, Ap. J. 234, 1105.

Lightman, A. 1981, Ap. J., in press.

Lovelace, R., MacAuslan, J., and Burns, M. 1979, Proceedings of La Jolla Institute Workshop on Particle Acceleration Mechanisms in Astrophysics, American Institute of Physics, New York, p. 399.

Lynden-Bell, D. 1969, Nature 223, 690.

MacDonald, D. and Thorne, K. 1981, Caltech preprint, OAP-616.

Marshall, F., Boldt, E., Holt, S., Miller, R., Mushotzky, R., Rose, L.A., Rothschild, R., and Serlemitsos, P. 1980, Ap. J. 235, 4.

Matteson, J., Gruber, D., Nolan, P., Peterson, L., and Kinzer, R. 1979, Bull. AAS 11, 653.

McKee, J., Mushotzky, R., Boldt, E., Holt, S., Marshall, F., Pravdo, S., and Serlemitsos, P. 1980, Ap. J. 242, 843.

Mushotzky, R., Marshall, F., Boldt, E., Holt, S., and Serlemitsos, P. 1980, Ap. J. 235, 377.

Mushotzky, R., and Marshall, F. 1980, Ap. J. 239, L5.

Mushotzky, R. 1982, Ap. J., in press.

Mushotzky, R., Serlemitsos, P., Smith, B., Boldt, E., and Holt, S. 1978, Ap. J. 225, 21.

Novikov, D., and Thorne, K. 1973, "Black Holes" (edited by C. and B. DeWitt), Gordon and Breach, New York, p. 343.

Osmer, P.S. 1981, Ap. J., submitted.

Perotti, F. et al. 1979, Nature 282, 484.

Perotti, F., Della Ventura, A., Villa, G., DiCocco, G., Bassani, L., Butler, R., Carter, J., and Dean, A. 1981a, Ap. J. 247, L63.

Perotti, F., Della Ventura, A., Villa, G., DiCocco, G., Butler, R., Carter, J., and Dean A. 1981b, Nature 292, 133.

Peterson, L., Rothschild, R., Baity, W., Matteson, J., Worrall, D., Primini, F., Dil, S., and Levine, A. 1981, Bull. APS 26, 583.

Piccinotti, G., Mushotzky, R., Boldt, E., Holt, S., Marshall, F., and Serlemitsos, P. 1982, Ap. J. , in press, Jan.

Rees, M., Begelman, M., Blandford, R., and Phinney, E. 1982, Nature 295, 17.

Rothschild, R. et al. 1981, in preparation.

Ruffini, R., and Wheeler, J. 1975, "Neutron Stars, Black Holes and Binary X-ray Sources" (edited by H. Gursky and R. Ruffini), Reidel: Dordrecht, p. 389.

Ryan, M.P. 1972, Ap. J. 177, L79.

Sanders, R. 1981, Nature 294, 427.

Schmidt, M. 1978, Physica Scripta 17, 135.

Schmidt, M., and Green, R. 1980, IAU Symposium 92, Objects of High Redshift (edited by G. Abell and P.J.E. Peebles) Reidel: Dordrecht, p. 73.

Schmidt, M. and Green, R. 1981, Vatican Study Week on Cosmology and Fundamental Physics.

Serlemitsos, P. 1981, Goddard Workshop on X-ray Astronomy and Spectroscopy.

Setti, G., and Rees, M. 1979, "Non-solar X- and Gamma-ray Astronomy", IAU Symposium 37 (D. Reidel:Dordrecht), p. 57.

Shapiro, S., Lightman, A., and Eardley, D. 1976, Ap. J. 204, 187.

Shields, C., and Mushotzky, R. 1979, Astr. Ap. 79 , 56.

Silk, J. 1970, Space Science Reviews 11, 671.

Simkin, S., Su, H., and Schwarz, M. 1980, Ap. J. 237, 404.

Stottlemyer, A. 1979, private communication.

Tennant, A., Mushotzky, R., Boldt, E., and Swank, J. 1981, Ap. J. 251, 15.

Tennant, A. et al. 1982, in preparation.

Terrell, J. 1977, American Journal of Physics 45, 869.

Thorne, K. 1974, Ap. J. 191, 507.

Trombka, J., Dyer, C., Evans, L., Bielefeld, M., Seltzer, S., and Metzger, A. 1978, Ap. J. 212, 925.

Tucker, W. 1967, Ap. J.148, 745.

Ulmer, M. et al. 1981, Ap. J. 243, 681.

Vestrand, W., Scott, J., Marsher, A., and Christiansen, W. 1981, Ap. J. 245, 811.

Webber, W., Lockwood, J., and Simpson, G. 1981, Conference Papers, 17th International Cosmic Ray Conference (Paris) Vol. 1, p. 247.

Weinberg, S. 1972, Gravitation and Cosmology (Wiley, New York).

Weisskopf, M. 1981, Proceedings, Wash. Acad. of Sci. 71, 69.

White, R.S., Dayton, B., Gibbons, R., Long, J.L., Zanrosso, E.M. and Zych, A.D. 1980, Nature 284, 608.

Worrall, D., Boldt, E., Holt, S., and Serlemitsos, P. 1980, Ap. J . 240, 421.

Worrall, D., Boldt, E., Holt, S., Mushotzky, R., and Serlemitsos, P. 1981, Ap. J. 243, 53.

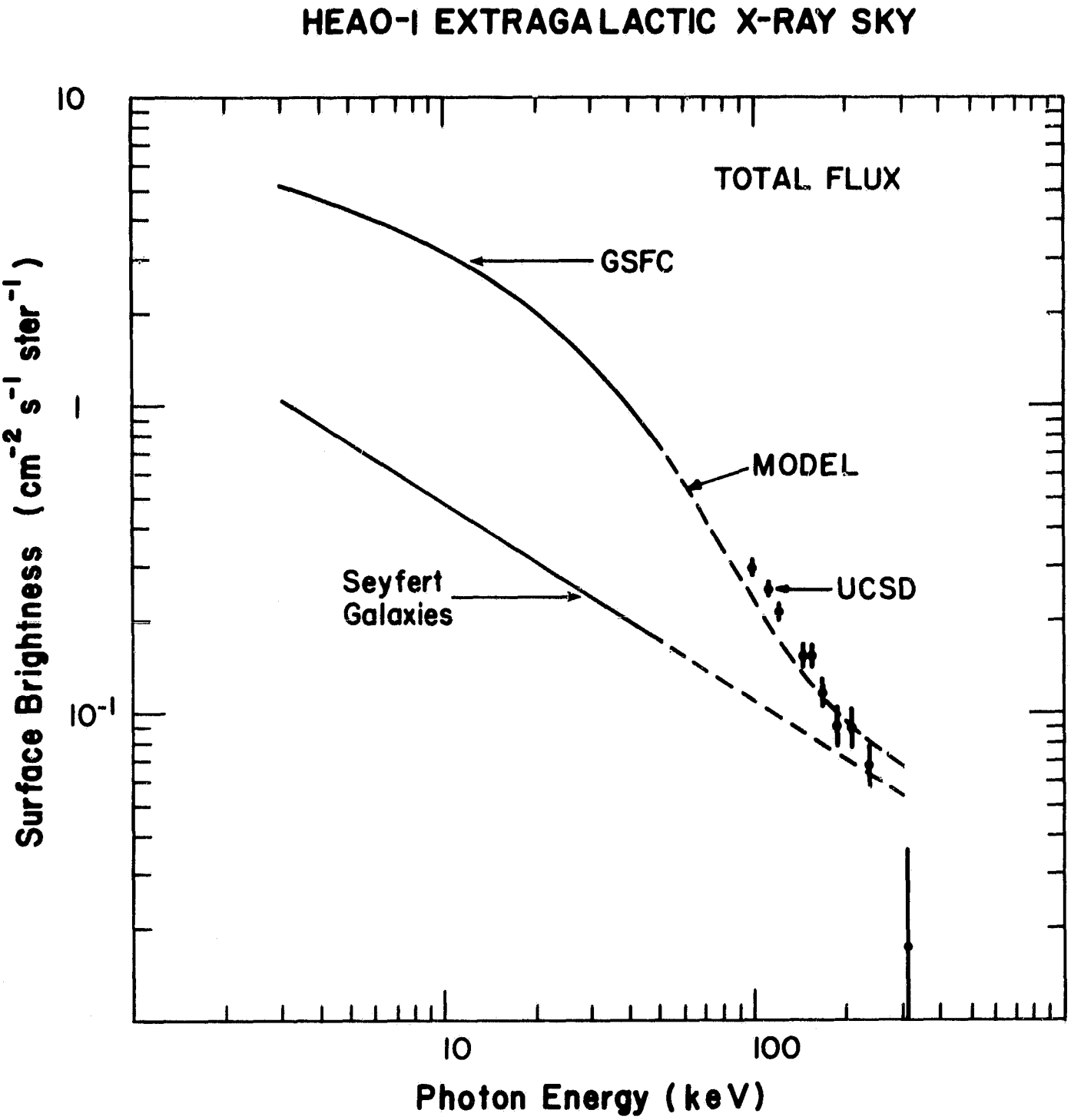
HEAO-1 EXTRAGALACTIC X-RAY SKY
TOTAL FLUX
GSFC
MODEL
UCSD
Seyfert
Galaxies
10
1
10⁻¹
Surface Brightness (cm⁻² s⁻¹ ster⁻¹)
10
100
Photon Energy (keV)

Figure 1

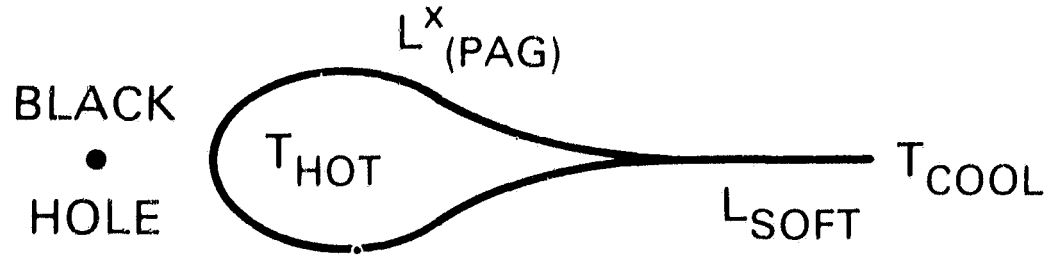


PAG ACCRETION DISK "WITH $e^{\pm}$ COOLING"

(A)

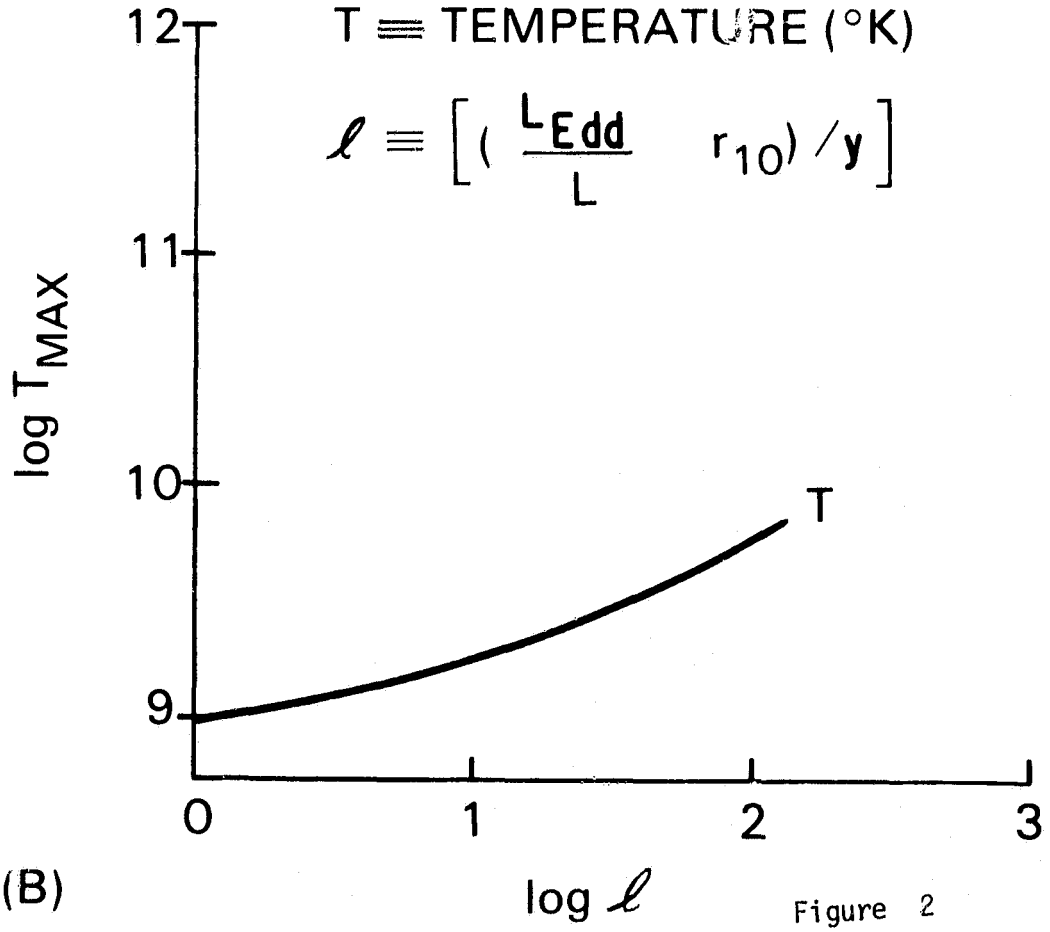


(B)

Figure 2

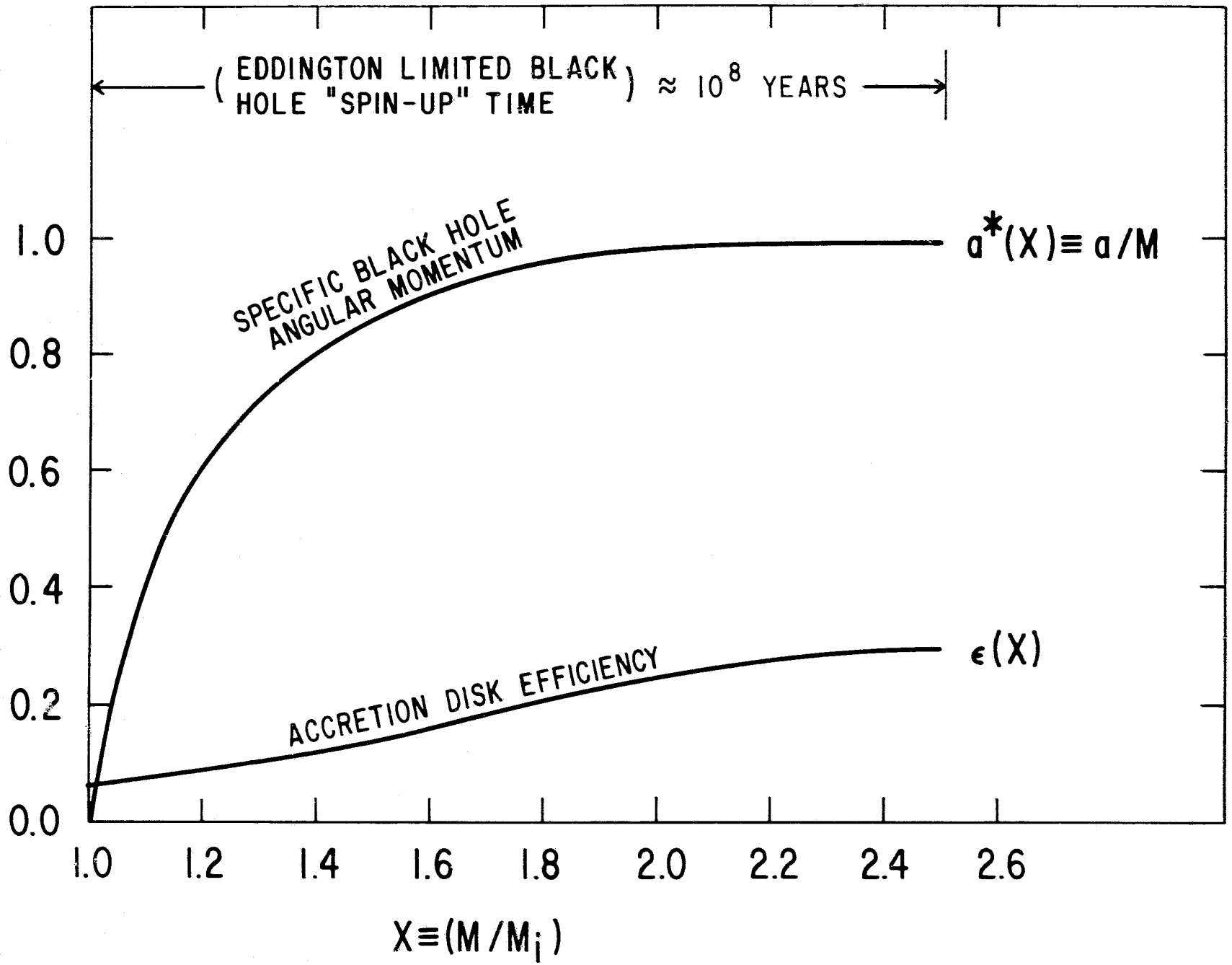
( EDDINGTON LIMITED BLACK HOLE "SPIN-UP" TIME ) ≈ 10^8 YEARS
SPECIFIC BLACK HOLE ANGULAR MOMENTUM
a*(X)≡a/M
ACCRETION DISK EFFICIENCY
ε(X)
1.0
0.8
0.6
0.4
0.2
0.0
1.0
1.2
1.4
1.6
1.8
2.0
2.2
2.4
2.6
X≡(M/M_i)

Figure 3

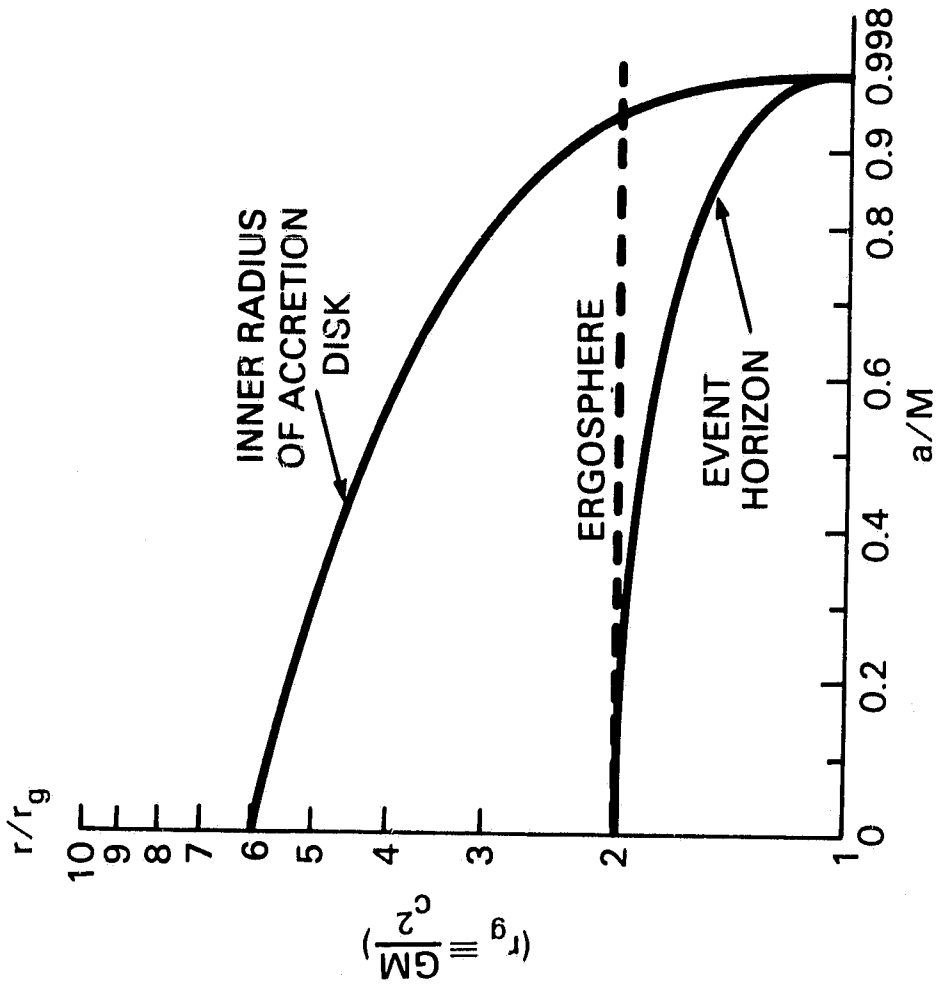
INNER RADIUS
OF ACCRETION
DISK
ERGOSPHERE
EVENT
HORIZON
r/r_g
10
9
8
7
6
5
4
3
2
1
0
0.2
0.4
0.6
0.8
0.9
0.998
a/M
(r_g ≡ GM/c²)

Figure 4

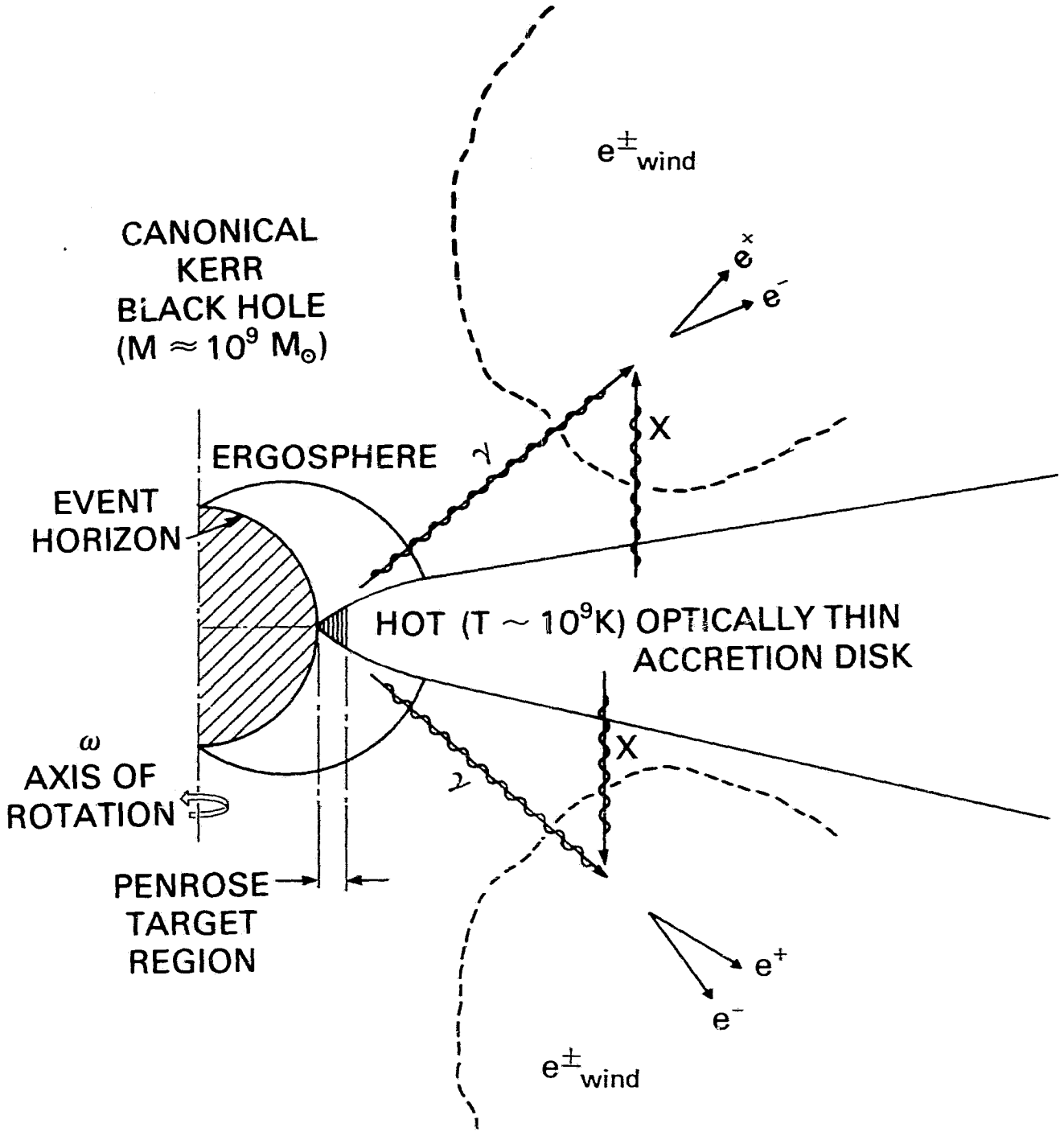
$e^{\pm}_{wind}$
CANONICAL
KERR
BLACK HOLE
($M \approx 10^9 M_\odot$)
$e^{\times}$
$e^-$
X
ERGOSPHERE
EVENT
HORIZON
HOT ($T \sim 10^9$K) OPTICALLY THIN
ACCRETION DISK
X
$\omega$
AXIS OF
ROTATION
PENROSE
TARGET
REGION
$e^+$
$e^-$
$e^{\pm}_{wind}$

Figure 5

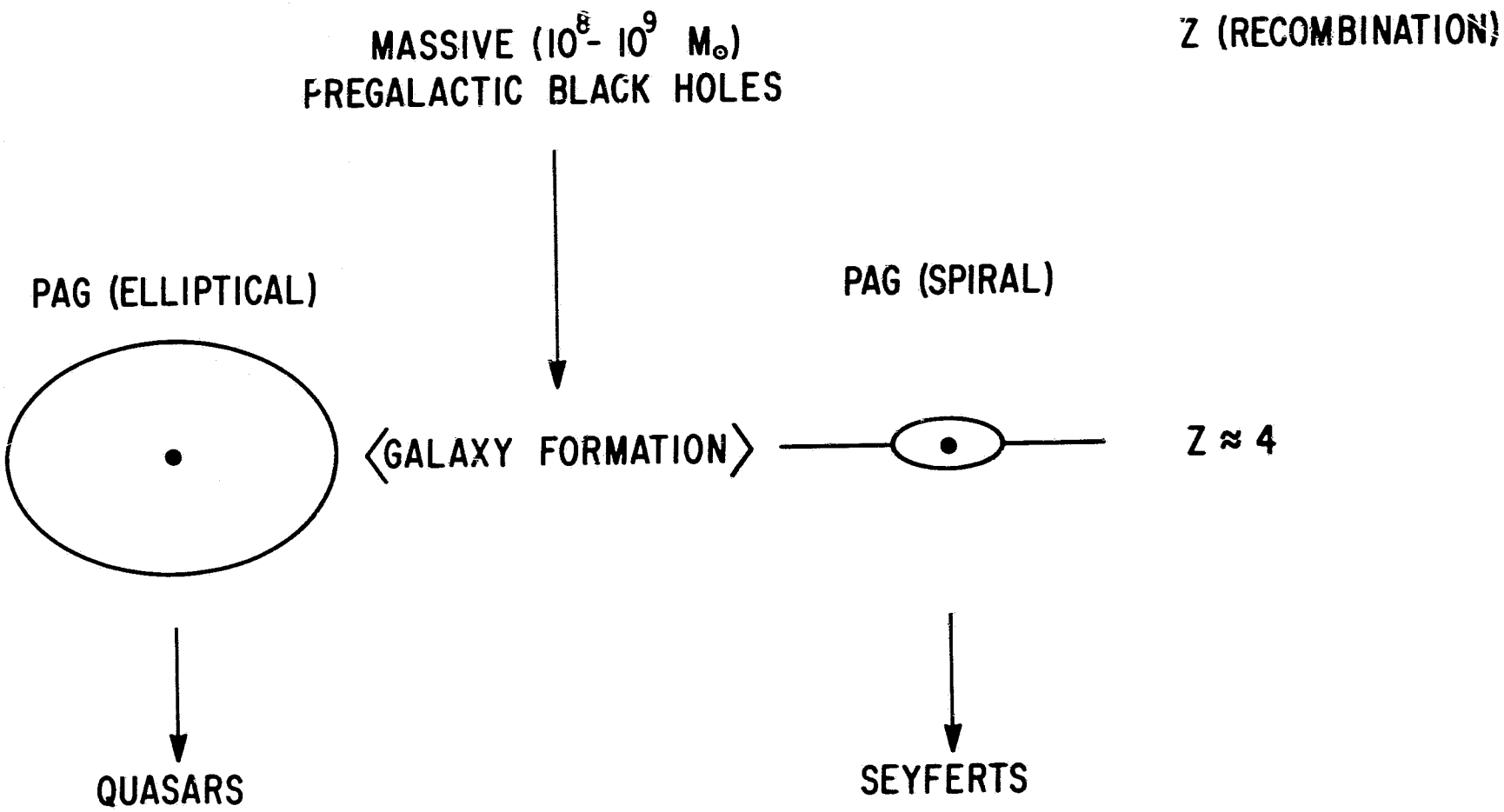
MASSIVE ($10^8$ - $10^9$ $M_\odot$)
PREGALACTIC BLACK HOLES
Z (RECOMBINATION)
PAG (ELLIPTICAL)
PAG (SPIRAL)
⟨GALAXY FORMATION⟩
Z ≈ 4
QUASARS
SEYFERTS

Figure 6

## EVOLUTION OF MASSIVE COMPACT OBJECTS

## $\sigma \equiv$ SURFACE DENSITY ON CELESTIAL SPHERE

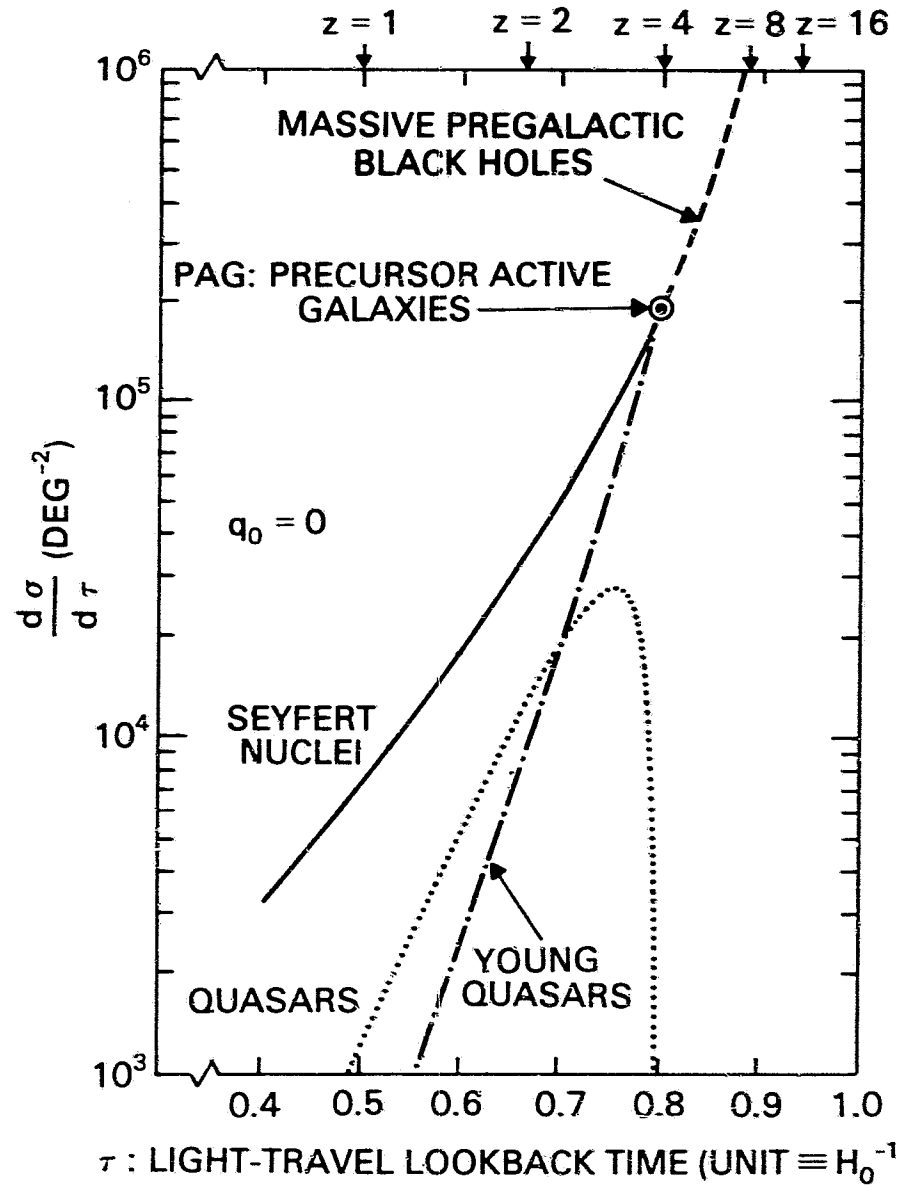


Figure 7

EVOLUTION OF MASSIVE COMPACT OBJECTS

$\sigma \equiv$ SURFACE DENSITY ON CELESTIAL SPHERE

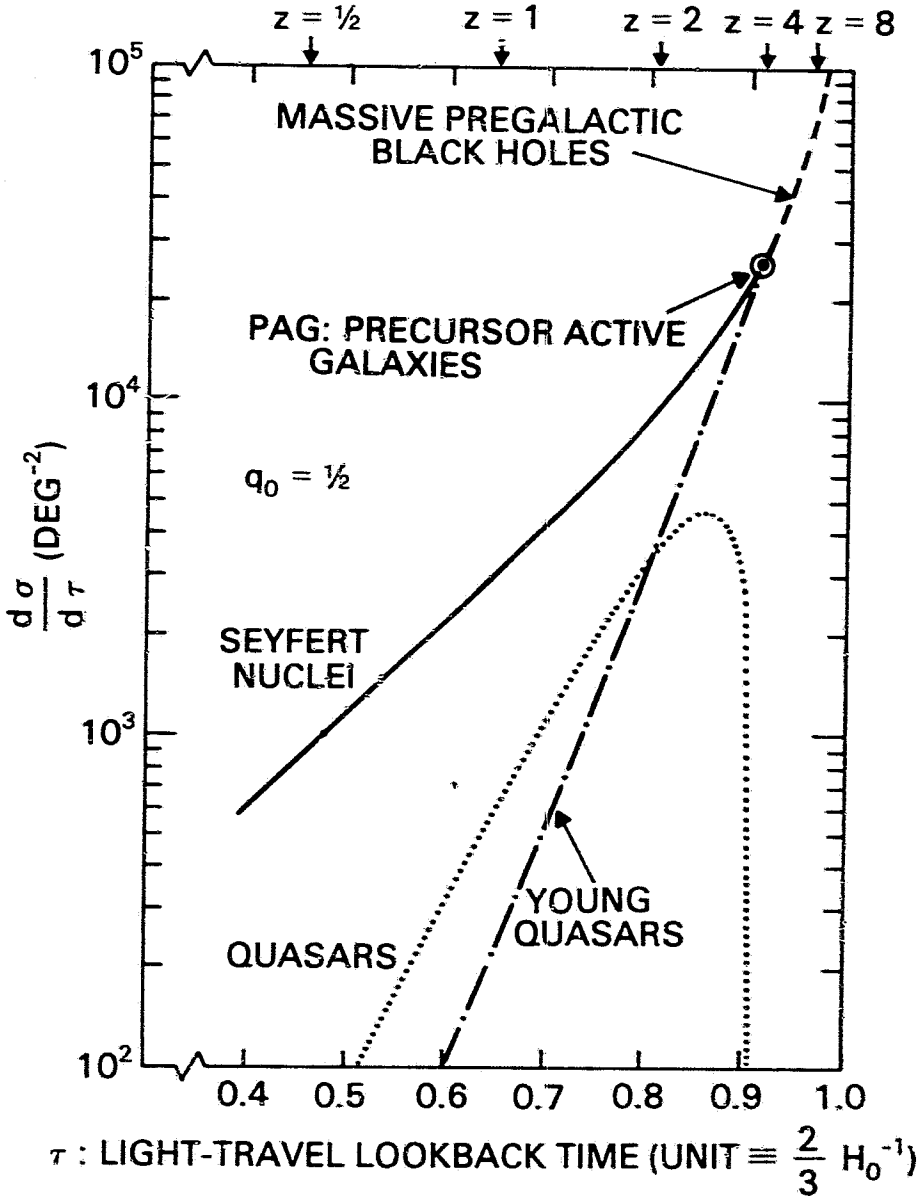


Figure 8

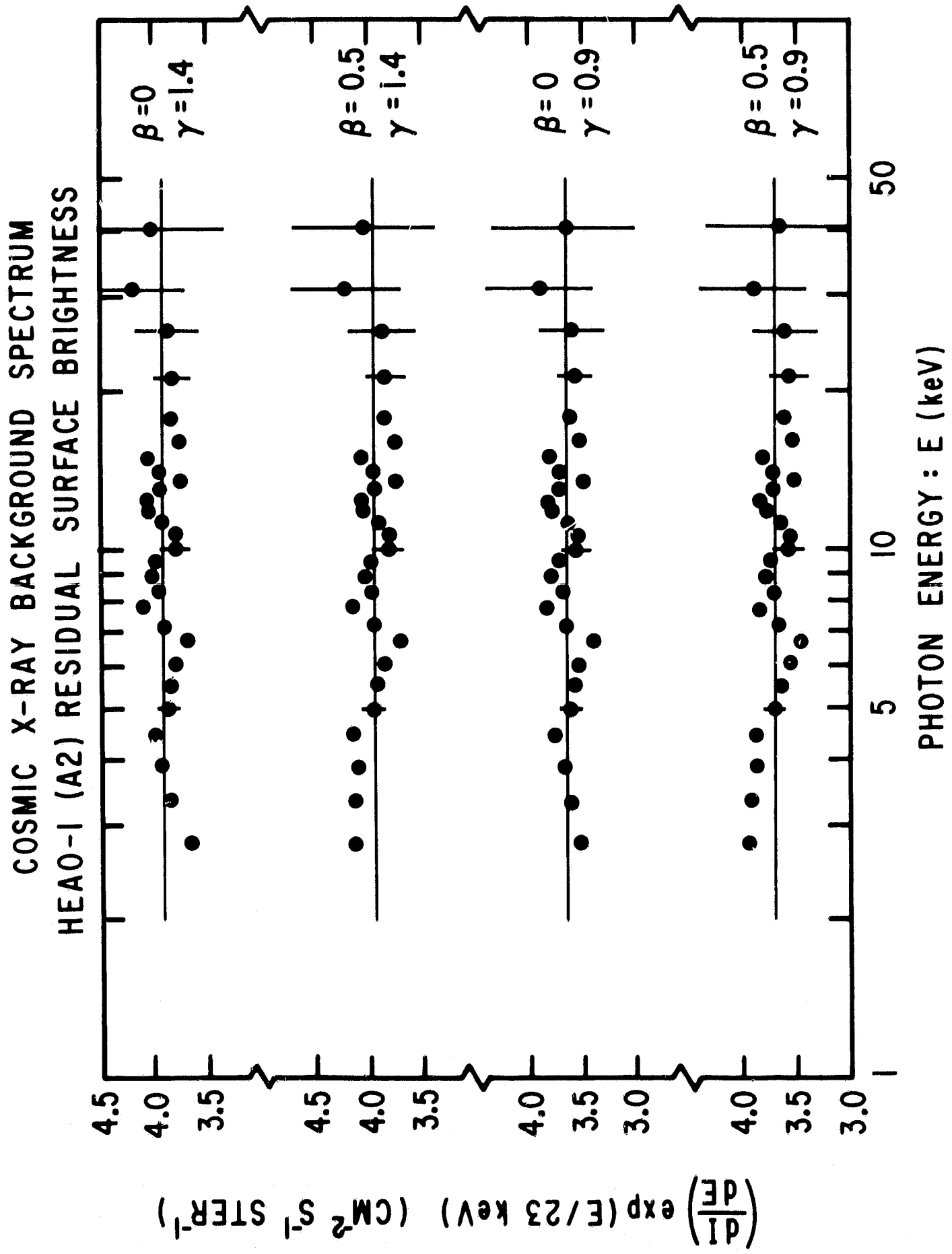
COSMIC X-RAY BACKGROUND SPECTRUM
HEAO-1 (A2) RESIDUAL SURFACE BRIGHTNESS
β=0 γ=1.4
β=0.5 γ=1.4
β=0 γ=0.9
β=0.5 γ=0.9
4.5
4.0
3.5
3.0
1
5
10
50
PHOTON ENERGY : E (keV)
$\left(\frac{dI}{dE}\right)$ exp (E/23 keV) (CM$^2$ S$^{-1}$ STER$^{-1}$)

Figure 9